Journal of Building Engineering 111 (2025) 113558

Contents lists available at ScienceDirect

Journal of Building Engineering

journal homepage: www.elsevier.com/locate/jobe

Code-based ground motion selection and scaling for seismic assessment: Application to two masonry building case studies

Daniel Caicedo [a,*], Igor Tomić [b], Shaghayegh Karimzadeh [a], Vasco Bernardo [c], Katrin Beyer [b], Paulo B. Lourenço [a]

[a] University of Minho, ISISE, ARISE, Department of Civil Engineering, Guimarães, Portugal
[b] École Polytechnique Fédérale de Lausanne (EPFL), Earthquake Engineering and Structural Dynamics Laboratory (EESD), Lausanne, Switzerland
[c] Earthquake Engineering and Structural Dynamics Unit (Structures Department), National Laboratory for Civil Engineering (LNEC), Lisbon, Portugal

ARTICLE INFO

Keywords:
Old masonry buildings
Eurocode 8
Ground motion selection and scaling
Non-linear analysis
Out-of-plane (OOP) response

ABSTRACT

This paper investigates the applicability and limitations of the guidelines for ground motion selection and scaling provided in the first- and second-generation of Eurocode 8 for the assessment of two unreinforced masonry buildings subjected to bi-directional loading. The numerical case studies consist of two unreinforced masonry buildings: one representative of stiff, monumental structures, and the other characterising tall, slender masonry typologies. Both structures are modelled in OpenSees using three-dimensional macroelements to capture the in-plane (IP) and out-of-plane (OOP) mechanisms, while also incorporating the effects of non-linear floor-to-wall connections and wall-to-wall interlocking. A total of ten sets of accelerograms are defined following the code-based requirements. These suites of accelerograms differ according to the version of Eurocode 8, seismological constraints, the range of matching, and the matching strategy, either uniform scaling or spectral matching. In addition to the bedrock case, soil classes B and C, defined according to Eurocode 8 prescriptions, are investigated. Subsequently, non-linear time history analyses are conducted for each building. The non-linear response obtained after the action of each set is thoroughly analysed in terms of mean and dispersion. Furthermore, the minimum number of records recommended in the code to characterise the mean seismic demand and its dispersion is examined. Finally, important remarks are drawn regarding ground motion selection and scaling guidelines, specifically oriented to the case of old masonry constructions.

1. Introduction

Old masonry constructions denote a major part of the building stock in Europe's historic centres [1]. On top of that, many of them are representative landmarks of cultural heritage whose preservation is imperative for the development and growth of social-economic activity. Particularly, these kinds of buildings are highly vulnerable to seismic damage mainly due to their exposure in regions with medium to major seismic hazard levels [2] in addition to their inherent characteristics, including the mechanical properties (*i.e.*, low tensile strength, low ductility, poor energy dissipation capacity, etc.), irregular configuration, or geometric irregularities [3–6]. Because of that, elastic approaches like response spectrum analysis are likely to lead to unrealistic estimations. Thus, other techniques,

* Corresponding author.
E-mail address: dcaicedod@civil.uminho.pt (D. Caicedo).

https://doi.org/10.1016/j.jobe.2025.113558
Received 6 March 2025; Received in revised form 20 July 2025; Accepted 21 July 2025
Available online 23 July 2025
2352-7102/© 2025 The Authors. Published by Elsevier Ltd. This is an open access article under the CC BY license (http://creativecommons.org/licenses/by/4.0/).

such as non-linear static (either standard or multi-modal pushover) or non-linear response history analyses, are needed for proper seismic evaluation of pre-code masonry buildings. Thanks to the latest innovations and improvements in computing power, it is conceivable to assess complex structural systems through non-linear dynamic analyses accounting for potential sources of uncertainty stemming from material or structural modelling parameters [7] and record-to-record variability [8]. Among these sources of uncertainty, the latter has shown a significant influence on the variability of structural response [9,10].

In this sense, the selection and scaling of ground motion records have been recognised as a major source of bias and uncertainty in the assessment of engineering structures through non-linear dynamic analyses [11]. Two major state-of-the-art reviews have presented the principal methodologies for the selection of 'appropriate' sets of records to be used for the dynamic analysis of structural systems, first by Katsanos et al. [12] and, more recently, by Caicedo et al. [11]. In general, both revisions addressed common topics including the selection and scaling of real records matching a target spectrum defined by code provisions or different targets such as the uniform hazard spectrum (UHS) [13,14] and the conditional mean spectrum (CMS) [15,16] along with selection of motions based on scalar or vector-valued intensity measures (IMs) for probabilistic assessment [17–22] and the usage of simulated signals as an alternative to ground motion selection and scaling [23–28]. Unfortunately, due to their large complexity or excessive time consumption, in the case of probabilistic approaches, almost none of the above-mentioned techniques are commonly used in conventional engineering practice. To overcome this limitation, seismic codes, such as Eurocode 8 [29], American Standards ASCE/SEI 41-13 [30] and ASCE/SEI 7–10 [31], or the New Zealand Standard NZS 1170.5:2004 [32], provided generalised guidelines to be adopted by practitioners for selection and scaling of input motions. Yet, there are few investigations available in the literature that address seismic safety-checking through code-compliant sets of records.

In line with investigating the effects of ground motion selection and scaling, Sextos et al. [33] quantified the impact of the Eurocode 8's approach on the structural performance of an existing irregular reinforced concrete (RC) building damaged during the Lefkada 2003 earthquake in Greece. Significant intra-set scatter was observed in the inelastic response, leading, in consequence, to an erroneous estimation of the mean response. Koboevic et al. [34] studied the influence of selection and scaling, matched to the UHS of the 2005 National Building Code of Canada (NBCC 2005) [35], on the median inelastic brace deformations of a four-story concentrically braced steel frame. After comparing the effect of amplitude-scaled historical records, the authors encouraged the implementation of source-based simulated records [36]. Likewise, Lin et al. [37] examined different methodologies to derive spectrum-compatible input records for the analysis of three building types ranging from low-medium to high-rise (*i.e.*, 4-, 10-, and 16-storey, respectively). On this occasion, the preference for real accelerograms, selected from earthquakes that occurred in regions with similar seismological characteristics to the target location and adequately scaled to match the design spectrum closely, was highlighted for performing time-history analyses of buildings. Michaud and Léger [38] evaluated the effectiveness of seven scaling methods and two spectral matching approaches using the NBCC 2005 UHS, considering both historical and simulated records. The results of non-linear dynamic analyses of various single-degree-of-freedom (SDOF) structures and a 4-storey steel frame revealed that spectral matching does not reduce the dispersion of the response, and its implementation is effective in reducing the number of records in seismic safety assessment.

Ergun and Ates [39] highlighted the large variability with respect to scaled sets of far-field and near-field ground motions following the criteria for time-domain scaling provided in ASCE 7-05 and Eurocode 8. Araújo et al. [40] compared code-based selection methods [29–32] with an emphasis on the number of records required for estimating the mean seismic response. An additional spectral mismatch limit (±50 %) was proposed for each record to reduce the record-to-record variability within the matching period range. This constraint was further described and mathematically supported in the research by Macedo and Castro [41], where SelEQ was introduced as a web-based tool for the selection and scaling of ground motion records. A similar formulation was presented more recently in the research by Kayhan et al. [42]. Reyes et al. [43] proposed an adjustment to the ASCE/SEI 7–10 scaling based on spectral shape and an additional scale factor applied to the entire record set, which led to significant improvements in estimating the structural response of multi-storey plan-asymmetric buildings. Karimzadeh et al. [44] investigated the effects of ASCE/SEI 7–16 and Eurocode 8 selection criteria on estimating the seismic demand of an unreinforced masonry shear wall. Eurocode 8-based selection led to higher demand in terms of global displacements. More recently, Jalayer et al. [45] pointed out that the average code-based safety-checking could end up being unconservative with respect to performance-based procedures because of epistemic uncertainties referred to as the record-to-record variability (*i.e.*, when the number of records is small).

This paper explores the seismic safety verification of old masonry buildings subjected to bi-directional loading while comparing the code-based guidelines for earthquake selection and scaling provided in the first- and second-generation Eurocode 8 [46]. Within this framework, mechanical and geometric uncertainties are disregarded in the study. Two unreinforced masonry constructions are adopted as case studies. The first one corresponds to a two-storey stiff monumental heritage structure, and the second is representative of tall and slender masonry residential buildings. The numerical modelling is carried out in OpenSees [47] using three-dimensional macroelements [48] to account for the in-plane (IP) and out-of-plane (OOP) mechanisms. The effects of non-linear floor-to-wall connections and wall-to-wall interlocking are also considered in the models [49]. After selecting key parameters for the definition of the target spectra, a total of ten sets of accelerograms are specified. These sets differ according to the version of Eurocode 8, seismological constraints, range of matching, and matching strategy (*i.e.*, uniform scaling, US, or spectral matching, SM). Like the study by Valente [50], which investigated the influence of spectrum-compatible accelerograms on the seismic response of historical masonry bell towers for different soil types, in this study, the effect of soil classes A, B, and C on the seismic response of unreinforced masonry constructions is investigated. The non-linear response obtained through time-history analyses is thoroughly investigated in terms of mean and dispersion for each set and soil class. Based on previous results from performance-based assessment [51], this research seeks to answer whether the minimum number of records recommended in the code is a reasonable assumption for the characterisation of the mean seismic demand and its dispersion. Lastly, important remarks are drawn, based on the findings of this research, concerning

the ground motion selection and scaling oriented to the safety-checking of unreinforced masonry buildings.

2. Overview of the numerical case studies

In this study, two old masonry buildings are adopted as case studies. Both structures were first analysed by Tomić et al. [7] and extended in the research by Caicedo et al. [51,52]. The numerical models of the buildings developed in OpenSees [47] are available in the online repository https://doi.org/10.5281/zenodo.12531709. Next, a brief description of the buildings' topology and general assumptions for the modelling strategy are provided.

2.1. Description of the buildings' topology

The Holsteiner Hof building is a 2-storey stone masonry building representative of stiff monumental heritage structures. According to the Swiss Inventory of Cultural Property of National and Regional Significance, this building is a landmark of cultural heritage. The plan of the building is regular, with dimensions of 26.00 m × 14.00 m. The height of each storey is 4.50 m. Wall and spandrel thicknesses are 0.60 m and 0.30 m, respectively. Gables at the top have a thickness of 0.45 m. The floor system is composed of timber beams, simply supported on the walls in the shorter direction, and a layer of planks nailed directly to the beams. Consequently, horizontal forces are transferred as friction forces. The roof system is composed of a wooden truss structure. Minor retrofitting interventions were reported during the period 1976–1979 without significant modifications to the structural system.

On the other side, the Lausanne Malley is a 6-storey structure representative of tall and slender masonry residential buildings. The building is regular in plan with dimensions of 14.00 m × 12.00 m. The storey height varies between 2.80 and 3.20 m, while the wall thickness gradually decreases from 0.60 to 0.25 m with the increasing of the building height. As with the Holsteiner Hof, the floor system is composed of timber beams, simply supported on the walls in the shorter direction, and a layer of planks nailed directly to the beams. The roof system is composed of a wooden truss structure. Soundproofing retrofitting measures were implemented recently and reported by Michel et al. [53]. The description of the two masonry building case studies is summarised in Table 1.

2.2. Modelling approach

Both buildings are idealised through the equivalent frame model (EFM) approach by discretising façades into piers, spandrels, and rigid nodes using beams or macroelements [54,55]. The numerical models are carried out in OpenSees [47] using the recent macroelement formulation by Vanin et al. [48] to account for the IP and OOP mechanisms. The macroelement is formulated as a one-dimensional element with two nodes at the element ends and one additional node at the midspan. It can capture the IP and OOP response through three sectional models applied at the element ends and at the central section (See Fig. 1a). P-Δ formulation is selected as geometric transformation in OpenSees to capture second-order non-linear effects. Drift values are calculated individually for flexural and shear deformations based on the rotations and lumped shear deformations at the central node. Exceeding the limits in drift values will lead to the loss of lateral strength of the element.

The floor system is modelled using orthotropic elastic membranes with higher stiffness in the direction of the beam span and lower stiffness in the perpendicular direction (i.e., membrane definition is given by the two moduli of elasticity in the orthogonal directions, shear modulus, and thickness of the diaphragm). The roof truss structure is not explicitly modelled, similar to the floor system, elastic membrane elements with an adequate roof pitch are implemented and assumed to transmit only vertical loads to the underlying walls. Non-linear floor-to-wall connections are modelled through zero-length elements and a simple material model for frictional interfaces. Sliding is allowed in the perpendicular direction to the wall, ruled by a friction coefficient, μ, and no cohesion, as shown in Fig. 1b. The material can fail and lead to the loss of load-bearing capacity if a maximum slip is exceeded in the positive local "y" direction. The beam pounding effect is modelled when the relative slip in the negative direction "y" or in any direction "z" direction exceeds a predefined "gap" threshold. The failure of the connection at the beam support can lead to the OOP failure of a pier element. Similarly, wall-to-wall interlocking is modelled through zero-length elements following a uniaxial material law to simulate the formation of vertical cracks and separation of the orthogonal walls, which might trigger the OOP failure of macroelements. Fig. 1c depicts the material's linear elastic behaviour in compression without crushing, and a finite tensile strength followed by exponential softening.

As in Caicedo et al. [51], material and modelling parameters are deterministic and taken either from the mean of a normal distribution or the median of a lognormal distribution from various experimental campaigns reported in [7]. For simplicity, those values

Table 1
Description of the buildings' topology.

Building	*Holsteiner Hof*	*Lausanne Malley*
General	Stiff monumental heritage structure	Tall and slender residential masonry building
N° storeys	2	6
Dimensions in plan	26.00 m × 14.00 m	14.00 m × 12.00 m
Storey height	4.50 m	3.20–2.80 m
Wall thickness	0.60–0.30 m	0.60–0.25 m
Floor system	Timber beams and planks	Timber beams and planks
Roof system	Secondary wooden truss structure	Secondary wooden truss structure
Retrofit	Minor during 1976–1979	Soundproofing and seismic performance [53]

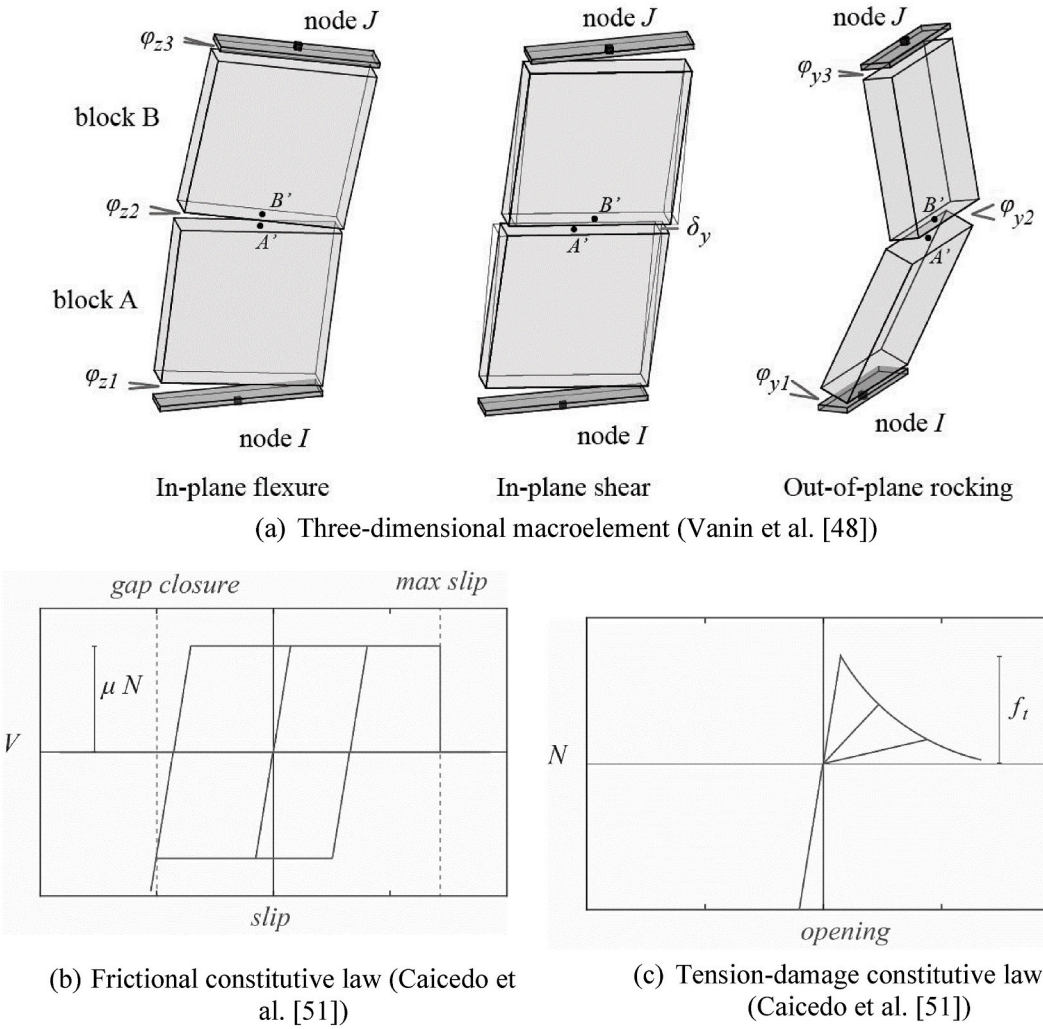


Fig. 1. General assumptions for the modelling strategy.

are summarised in Table 2. The drift capacities in flexure and shear, $\delta_{C,flexure}$ and $\delta_{C,shear}$, represent the ultimate flexural and shear drift limits at which the lateral stiffness of the macroelement is set to zero, as defined by Vanin et al. [56]. The Rayleigh damping model is assumed for response-history analyses, proportional to mass and secant stiffness, and calibrated at 5 % on the first and sixth frequencies for both buildings. The secant-stiffness approach introduces a correction term to the initial stiffness matrix used in the classical

Table 2
Material and modelling parameters (Caicedo et al. [51,52]).

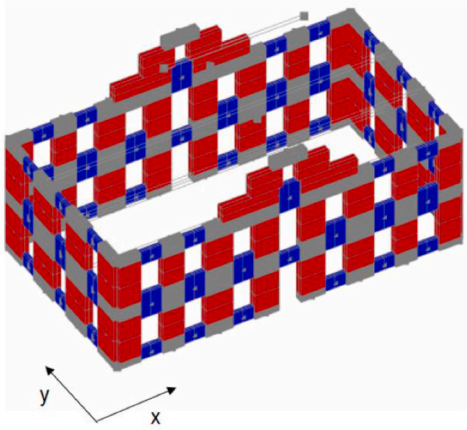
Parameter	Unit	Definition	Mean value
Masonry Parameters			
E_m	[Pa]	Modulus of elasticity [61–63]	3.5×10^9
G_m	[Pa]	Shear modulus [61–63]	$1.5 \times 10^{9*}$
f'_{cm}	[Pa]	Compressive strength [61–63]	1.3×10^6
c_m	[Pa]	Cohesion [61–63]	$2.3 \times 10^{5*}$
μ_m	[−]	Friction coefficient [61–63]	0.25*
ρ	[kg/m^3]	Density [61–63]	2000
Modelling Parameters			
$\delta_{C,flexure}$	[−]	Drift capacity in flexure [56]	0.01035*
$\delta_{C,shear}$	[−]	Drift capacity in shear [56]	0.007*
ζ	[−]	Damping ratio [49]	0.05

Note: (*) median value taken from a lognormal distribution.

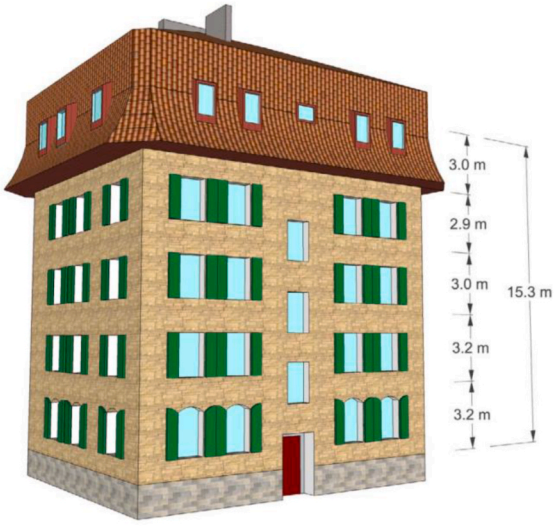
Rayleigh damping. This approach approximates the behaviour of the secant-stiffness proportional damping model, with the correction term being updated at each converged analysis step. By employing secant-stiffness proportional damping, the model achieves a more accurate simulation of OOP rocking behaviour, closely aligning with experimental data and classical rocking formulations [57,58]. A 5 % damping ratio was also adopted in previous studies by Caicedo et al. [51,52], based on the consideration that the damping ratio of masonry structures increases with damage, compared to the undamaged state, which has been experimentally shown to be around 3 % [59,60]. An additional aspect influencing the OOP dynamic response of the macroelement is the damping model, which governs energy dissipation during rocking oscillations. The macroelement accounts for dissipative phenomena at the sectional level, and through viscous and numerical damping. Since significant crushing at the section edge does not occur under moderate axial loads, the dissipative behaviour during rocking oscillations is primarily attributed to damping mechanisms rather than material failure [48]. Fig. 2 shows the numerical modelling implementation of the Holsteiner Hof and Lausanne Malley buildings. The fundamental vibration periods of the structures that will be needed subsequently for earthquake selection in Section 3.4 are 0.16 s and 0.50 s for the Holsteiner Hof and Lausanne Malley buildings, respectively.



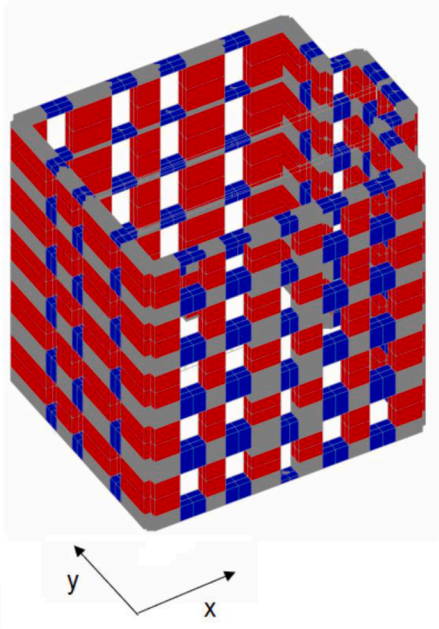
(a) Holsteiner Hof, main façade.



(b) Holsteiner Hof, numerical model.



(c) Lausanne Malley, scheme (source Michel et al. [53]).



(d) Lausanne Malley, numerical model.

Fig. 2. Numerical modelling implementation.

3. Ground motion selection and scaling strategies

This study aims to contrast the guidelines provided in the "EN 1998-1-1:2004" and the latest "EN 1998-1-1:2024" of the Eurocode 8, Part 1, for the alternative representation of the seismic action using input motions for response history analysis. These differences lie in the definition of the elastic response spectra and the criteria for the selection and scaling of input motions. The following subsections provide a comparison of the elastic response spectra defined in the first- and second-generation of the Eurocode 8. Then, the rules for selection and scaling are summarised for both versions of the code, and the formulation of the algorithm for selection and scaling is presented. Lastly, the different suites of records are shown for each version of Eurocode 8, seismological constraints, range of matching, and matching.

3.1. Target elastic response spectrum

The elastic response spectrum, S_e, defined in EN 1998-1-1:2004 [29] for the horizontal components of the seismic action is given in Fig. 3a, and defined by:

$$S_e(T) = \begin{cases} a_g S\left[1 + \dfrac{T}{T_B}(\eta 2.5\text{-}1)\right]; if \;\; 0 \le T \le T_B \\ a_g S \eta 2.5 \;;\; if \; T_B \le T \le T_C \\ a_g S \eta 2.5\left[\dfrac{T_C}{T}\right] \;;\; if \; T_C \le T \le T_D \\ a_g S \eta 2.5\left[\dfrac{T_C T_D}{T^2}\right] \;;\; if \; T_D \le T \le 4s \end{cases} \quad (1)$$

where T is the vibration period of a linear SDOF system; a_g is the design ground acceleration on type A ground, a_{gR}, multiplied by an importance factor γ_I; T_B and T_C are the lower and upper limits of the period in the constant spectral acceleration branch; T_D is the value defining the beginning of the constant displacement response range of the spectrum; S is the soil factor; and η is the damping correction factor with a reference value of $\eta = 1$ for 5 % viscous damping. The values of S, T_B, T_C, and T_D are tabulated within the code for the Type 1 spectrum (high-magnitude, distant earthquakes with strong energy release) and the Type 2 spectrum recommended when the earthquakes that contribute most to the seismic hazard have low-to-moderate surface-wave magnitude, M_s, not greater than 5.5; while the value of a_{gR} can be taken from peak ground acceleration (PGA) maps. In general, the shape defined in the present version of Eurocode 8, Part 1, is well-known and easy to reproduce by practitioners in the fields of structural and earthquake engineering.

Recently, the new standard shape depicted in Fig. 3b was introduced in the latest EN 1998-1-1:2024 version of Eurocode 8, Part 1. On this occasion, the definition of horizontal components of the seismic action relies on the estimation, from hazard maps of spectral accelerations for two periods, namely S_α (*i.e.,* maximum response spectral acceleration, for 5 % damping, at the constant acceleration range of the elastic response spectrum) and S_β (5 %-damped response spectral acceleration at the vibration period $T_\beta = 1$ s). The new S_e shape can be defined then by:

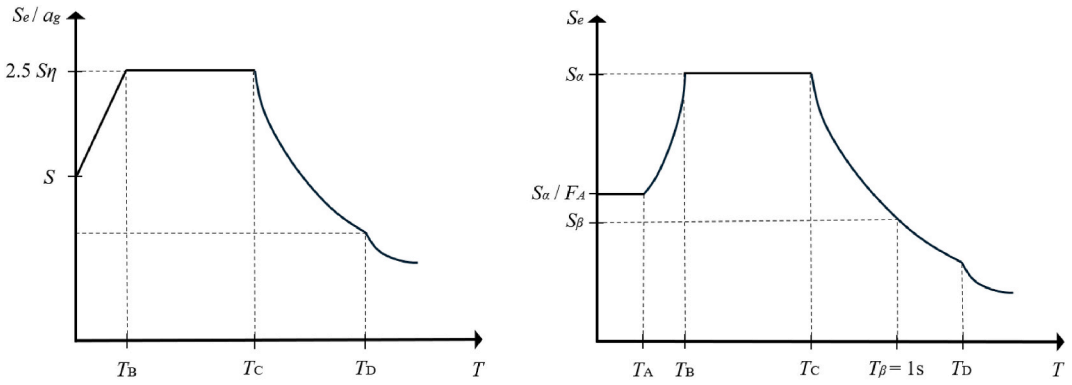


Fig. 3. Elastic response spectrum shape, Eurocode 8, Part 1.

$$S_e(T)=\begin{cases} \dfrac{S_\alpha}{F_A}\ ;\ if\ \ 0\le T<T_A \\ \dfrac{S_\alpha}{T_B\text{-}T_A}\left[\eta(T\text{-}T_A)+\dfrac{T_B\text{-}T}{F_A}\right]\ ;\ if\ T_A\le T<T_B \\ \eta S_\alpha\ ;\ if\ T_B\le T<T_C \\ \eta\dfrac{S_\beta T_\beta}{T}\ ;\ if\ T_C\le T<T_D \\ \eta T_D\dfrac{S_\beta T_\beta}{T^2}\ ;\ if\ \ T\ge T_D \end{cases} \tag{2}$$

$$S_\alpha = F_T F_\alpha S_{\alpha,RP} \tag{3}$$

$$S_\beta = F_T F_\beta S_{\beta,RP} \tag{4}$$

where F_T is the topography amplification factor; T_A is the short-period cut-off associated with the zero-period spectral acceleration (i.e., PGA); and F_A is the ratio of S_α to the zero-period spectral acceleration. Additionally, the corner frequency values can be calculated as:

$$T_B=\begin{cases} \dfrac{T_C}{x}\ ;\ if\ 0.05\ \text{s}\le\dfrac{T_C}{x}\le 0.10\ \text{s} \\ 0.05\ \text{s}\ ;\ if\ \dfrac{T_C}{x}<\ 0.05\ \text{s} \\ 0.10\ \text{s}\ ;\ if\ \dfrac{T_C}{x}>0.10\ \text{s} \end{cases} \tag{5}$$

$$T_C=\frac{S_\beta T_\beta}{S_\alpha} \tag{6}$$

$$T_D=\begin{cases} 2;\ if\ S_{\beta,RP}\le 1\ \text{m/s}^2 \\ 1+S_{\beta,RP}\ ;\ if\ S_{\beta,RP}\ >\ 1\ \text{m/s}^2 \end{cases} \tag{7}$$

Here, x is used to define the lower corner period, T_B, as a fraction of the upper one, T_C, which is defined in equation (6). The values of T_A, F_A, and x are tabulated for the definition of the standard elastic spectrum. Likewise, F_α and F_β, corresponding to the amplification factors in the short and intermediate periods, can be calculated according to the site category. Finally, the values of $S_{\alpha,RP}$ and $S_{\beta,RP}$ are taken directly from spectral acceleration maps. The new spectral shape provides a more consistent representation of the seismic action at a given location by accounting for the mapped characterisation of the seismic hazard. The site-specific seismic hazard evaluation is a key advantage of the new seismic code, leading to more reasonable evaluations of structural performance.

3.2. First-generation eurocode 8 guidelines

EN 1998-1-1:2004 established that the seismic motion may be represented in terms of ground acceleration time-histories. It is also specified that for three-dimensional analyses, the same accelerogram cannot be used simultaneously along both horizontal directions, and the description of the seismic motion may be made using artificial, recorded, or simulated accelerograms. The suite of accelerograms should meet the following conditions:

- A minimum of three accelerograms should be used.
- The mean of the zero-period spectral response acceleration values (calculated from the individual time histories) should not be smaller than the value of a_gS for the site in question.
- In the range of periods between $0.2T_1$ and $2T_1$, where T_1 is the fundamental period of the structure in the direction where the accelerogram will be applied, the mean 5 % damped elastic spectrum, calculated from all ground motion time histories, should not be less than 90 % of the corresponding value of the 5 % damped elastic response spectrum.

Moreover, section 4.3.3.4.3 of the code states that if the response is obtained from at least seven non-linear time-history analyses, the average of the response quantities from all these analyses should be assumed as the structural demand. Otherwise, the most unfavourable value of the response quantity among the analyses should be used.

3.3. Second-generation eurocode 8 guidelines

Unlike the previous version, Annex D, within the EN 1998-1-1:2024 edition, provides detailed criteria for the selection and scaling of input accelerograms for response-history analyses. The new code version explicitly mentions that the minimum number of input

motions may be reduced to three, considering the maximum response, only for low and very low seismic action classes, considering the most unfavourable peak response; otherwise, a minimum of seven sets of input motions must be used, and the average peak response should be considered for estimating the seismic action effects. Simulated and artificial accelerograms are both allowed in the EN 1998-1-1:2024 edition. Real ones are preferred in regions with available records from qualified strong-motion databases. Yet, ground motion simulations are encouraged in areas lacking seismic stations or having a limited history of large-magnitude and potentially destructive earthquakes. Furthermore, the selection should account, as far as possible, for the regional tectonic environment, earthquake magnitude (M_w), source-to-site distance, and local conditions of the recording site, relevant to the return period of the seismic actions of interest. Subsequently, the following numerical constraints can be identified in the Annex to the code:

- The spectral accelerations of the selected accelerograms should approach the elastic response spectrum in the matching range of 0.2 T_1 to 1.5 T_1.
- The scaling factor should not be larger than 2.0 nor smaller than 0.5 in the context of geotechnical applications or in the case of highly non-linear structural response.
- In the matching range $0.2T_1$—$1.5T_1$, the ratio of the average response spectrum to the target response spectrum should fall within the band from 0.75 to 1.3 and should have an average value larger than 0.95.
- In the matching range $0.2T_1$—$1.5T_1$, the individual spectrum of each accelerogram of the suite should not be out of the ±50 % of the target spectrum.
- The suite of motions should not contain simultaneously two components of the same record and no more than two records from the same earthquake.

These rules refer mainly to constant-amplitude or US scaling, in which the record is scaled in the time domain by a constant factor. Nevertheless, the second-generation guidelines allow for spectral-matching scaling, in which modifications are made in the frequency domain by adding wavelets until the response spectrum of the modified record approaches the target. Regarding multi-dimensional analyses, it is specified that compatibility of the horizontal components to the target spectrum should be verified based on the geometric mean of the horizontal spectral accelerations of records, and the orientation of the horizontal components with respect to the principal directions of the structure may be arbitrarily selected. It should be noted that as an alternative to the elastic response spectrum, UHS or CMS are allowed as targets. However, the present study focuses only on the comparison of the standard shapes proposed in both versions of the Eurocode 8, as depicted in Fig. 3.

3.4. Algorithm for selection and scaling

Past investigations [41,42,64–73] addressed the selection procedure of acceleration records for non-linear dynamic analysis as a constrained optimisation problem; among them, some tools have been widely adopted for ground motion selection in code-based seismic analysis, namely SelEQ [41] and REXEL [73]. Similarly, this study proposes a general algorithm that is easy to adapt to the conditions established in both versions of the Eurocode 8. In this regard, the sum of square differences between the mean of the suite of records and the target spectrum is defined as:

$$F(x) = \sum_{i=1}^{j} \left(S_{a,\mathrm{mean}}(T_i) \text{-} S_{a,\mathrm{target}}(T_i)\right)^2 \tag{8}$$

where j is equal to the number of vibration periods considered in the matching domain. $F(x)$ denotes the main objective for minimising to achieve convergence with the target design spectrum. Nonetheless, additional constraints should be taken into consideration to create a global optimisation problem with penalty functions. In the first place, lower and upper bounds for the mean spectrum can also be defined to generalise the first constraint in the form:

$$C_1(x) = \begin{cases} \textit{lower bound}_{\mathrm{mean}} - \min\left[S_{a,\mathrm{mean}}(T_i)/S_{a,\mathrm{target}}(T_i)\right];\ \textit{if } \min\left[S_{a,\mathrm{mean}}(T_i)/S_{a,\mathrm{target}}(T_i)\right] < \textit{lower bound}_{\mathrm{mean}} \\ \max\left[S_{a,\mathrm{mean}}(T_i)/S_{a,\mathrm{target}}(T_i)\right] - \textit{upper bound}_{\mathrm{mean}};\ \textit{if } \max\left[S_{a,\mathrm{mean}}(T_i)/S_{a,\mathrm{target}}(T_i)\right] > \textit{upper bound}_{\mathrm{mean}} \\ 0;\ \text{otherwise} \end{cases} \tag{9}$$

In that way, the $S_{a,\ \mathrm{mean}}(T)/S_{a,\ \mathrm{target}}(T)$ ratio is calculated, and a penalty cost is defined either as the difference between the lower bound for the mean spectrum and the minimum value of this ratio, or the difference between the maximum ratio with the upper bound of the mean spectrum, is added to the global optimisation problem in case that those minimum or maximum values of the ratio are out of the lower and upper bounds set for the mean spectrum. Analogously, a second constraint can be defined, this time for the lower and upper limits of each record:

$$C_2(\boldsymbol{x}) = \begin{cases} \textit{lower bound}_{\text{ind}} - \min\left[S_{a,\text{ind}}(T_i)/S_{a,\text{target}}(T_i)\right];\ \textit{if}\ \min\left[S_{a,\text{ind}}(T_i)/S_{a,\text{target}}(T_i)\right] < \textit{lower bound}_{\text{ind}} \\ \max\left[S_{a,\text{ind}}(T_i)/S_{a,\text{target}}(T_i)\right] - \textit{upper bound}_{\text{ind}};\ \textit{if}\ \max\left[S_{a,\text{ind}}(T_i)/S_{a,\text{target}}(T_i)\right] > \textit{upper bound}_{\text{ind}} \\ 0;\ \text{otherwise} \end{cases} \tag{10}$$

$C_2(\boldsymbol{x})$ will include an additional cost to the global optimisation problem every time that the $S_{a,\ \text{ind}}(T)/S_{a,\ \text{target}}(T)$ ratio is out of the bounds established for the individual spectrum. This constraint was originally proposed by Macedo and Castro [41] to reduce the individual mismatch, commonly referred to as the so-called record-to-record variability. Thus, the global optimisation problem assumes the final form:

$$F(\boldsymbol{x}) = \sum_{i=1}^{j} \left(S_{a,\text{mean}}(T_i) - S_{a,\text{target}}(T_i)\right)^2 + C_1(\boldsymbol{x}) + C_2(\boldsymbol{x}) \tag{11}$$

In the research listed above [41,42], an additional penalty is imposed when the same ground motion, or event, is considered more than once in the selected set. However, a different approach is adopted herein to decrease the complexity of the objective function by reducing the number of constraints within the global optimisation problem. First, a series of seismological conditions (*i.e.*, source mechanism, magnitude, source-to-site distance, and soil conditions) are considered to apply a first filter to the dataset of ground motion records. Then, the sum of squared errors (SSE) between the acceleration spectrum and the target spectrum is computed, considering the two main horizontal components of each record. Since this study focuses on the horizontal ground components affecting masonry buildings, the filtered set is reorganised by ranking the SSE of each record in the two directions of analysis from lowest to largest. To address the issue of selecting motions from the same record, only the component with the lowest SSE is retained for the next stage. Subsequently, to further resolve the same-event-record issue, records originating from the same event are excluded, conserving only the one with the highest (unscaled) compatibility with the target code spectrum.

After all mathematical formulation is set regarding the objective function and additional constraints, the vector **x** is introduced as:

$$\mathbf{x} = \{x_1, x_2 \cdots x_N\}^T \tag{12}$$

where the value of x_i denotes the ith scaling factor affecting the ith record in a set of N accelerograms in such a way that the $S_{a,\ \text{mean}}(T)$ is calculated as:

$$S_{a,\text{mean}}(T) = \frac{\sum_{i=1}^{N} S_{a,\text{ind}}(\mathrm{T})}{\mathrm{N}} \tag{13}$$

Therefore, the optimisation problem is now aimed at determining the x_i scaling factors that will reduce the total cost defined earlier in Equation (11), for which the differential evolution (DE) metaheuristic is adopted. This metaheuristic, introduced by Storn and Price [74], is part of evolutionary computing, and it is oriented to determine solutions for optimisation problems of real variables in continuous fields. A full description of the adaptation of the DE metaheuristic technique to a well-known civil engineering problem can be found in [75]. For the problem analysed herein, the conventional *'best1bin'* DE strategy is selected. The initial population is set to 100 random solution vectors, and the mutation and recombination constants are fixed as 0.5 and 0.4, respectively, for a maximum of 100 iterations.

3.5. Sets of records

The derived suites of records depend on the Eurocode 8 version in addition to the seismological constraints, range of matching, and matching strategy. The seismological constraints can be considered as "Fully" or "Relax". When the "Fully" flag is activated, all seismological constraints referred to source mechanism, M_w, Joyner-Boore distance (R_{JB}), and average shear wave velocity in the top

Table 3
Definition of the suites of records for non-linear time-history analyses.

Set	Version	Constraints	Domain	Strategy
1a	First-generation	Fully	Range	US
1b	Second-generation	Fully	Range	US
2a	First-generation	Relax	Range	US
2b	Second-generation	Relax	Range	US
3a	First-generation	Fully	Entire	US
3b	Second-generation	Fully	Entire	US
4a	First-generation	Relax	Entire	US
4b	Second-generation	Relax	Entire	US
5a	First-generation	Fully	Entire	SM
5b	Second-generation	Fully	Entire	SM

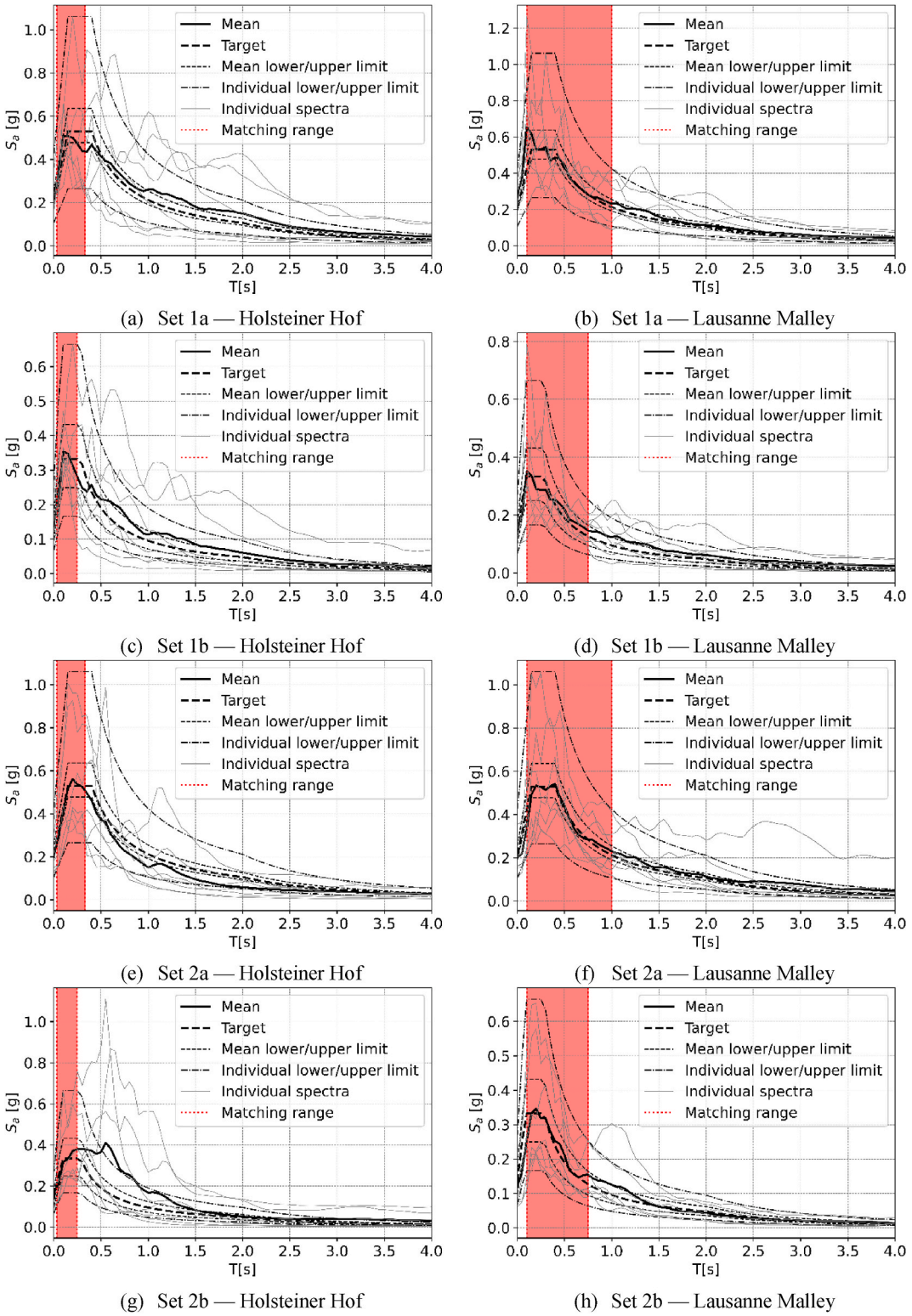


Fig. 4. Sets of records — Soil type A.

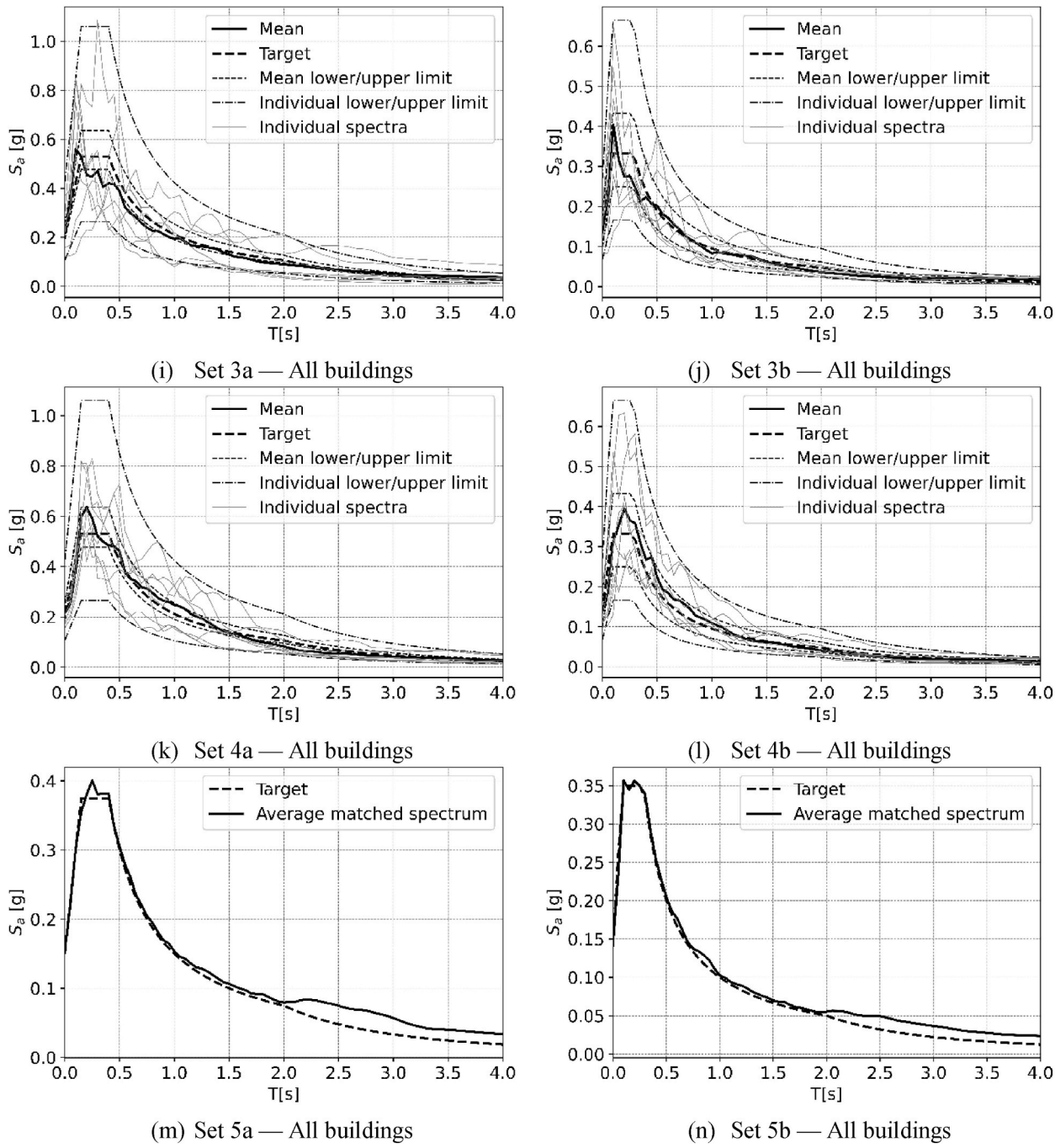


Fig. 4. (*continued*).

30 m of soil (V_{S30}) are accounted for to preselect the suitable suite of motions. On the contrary, only M_w and R_{JB} are considered if seismological constraints are set as "Relax". The matching range, on the other hand, refers to $0.2T_1$–$2T_1$ and $0.2T_1$–$1.5T_1$ for the previous and most recent versions of the Eurocode 8, respectively. In this sense, the selection depends on the fundamental period of the structure, and it is independent for each building. Additionally, the effect of improving the compatibility with the target spectrum across the entire period domain will be examined. The matching range is indicated in the "Domain" column, where "Range" refers to the standard-defined intervals ($0.2T_1$–$2T_1$ or $0.2T_1$–$1.5T_1$), and "Entire" denotes a broader matching domain extending up to $T = 4.0$ s. Lastly, the matching strategy refers to constant-amplitude US or SM. For the latter, the academic version of SeismoMatch v2024 is used. This software adopts the wavelets algorithm proposed by Abrahamson [76] and Hancock et al. [77] to match a specific target response spectrum. Accordingly, a total of ten sets of accelerograms are defined and summarised in Table 3.

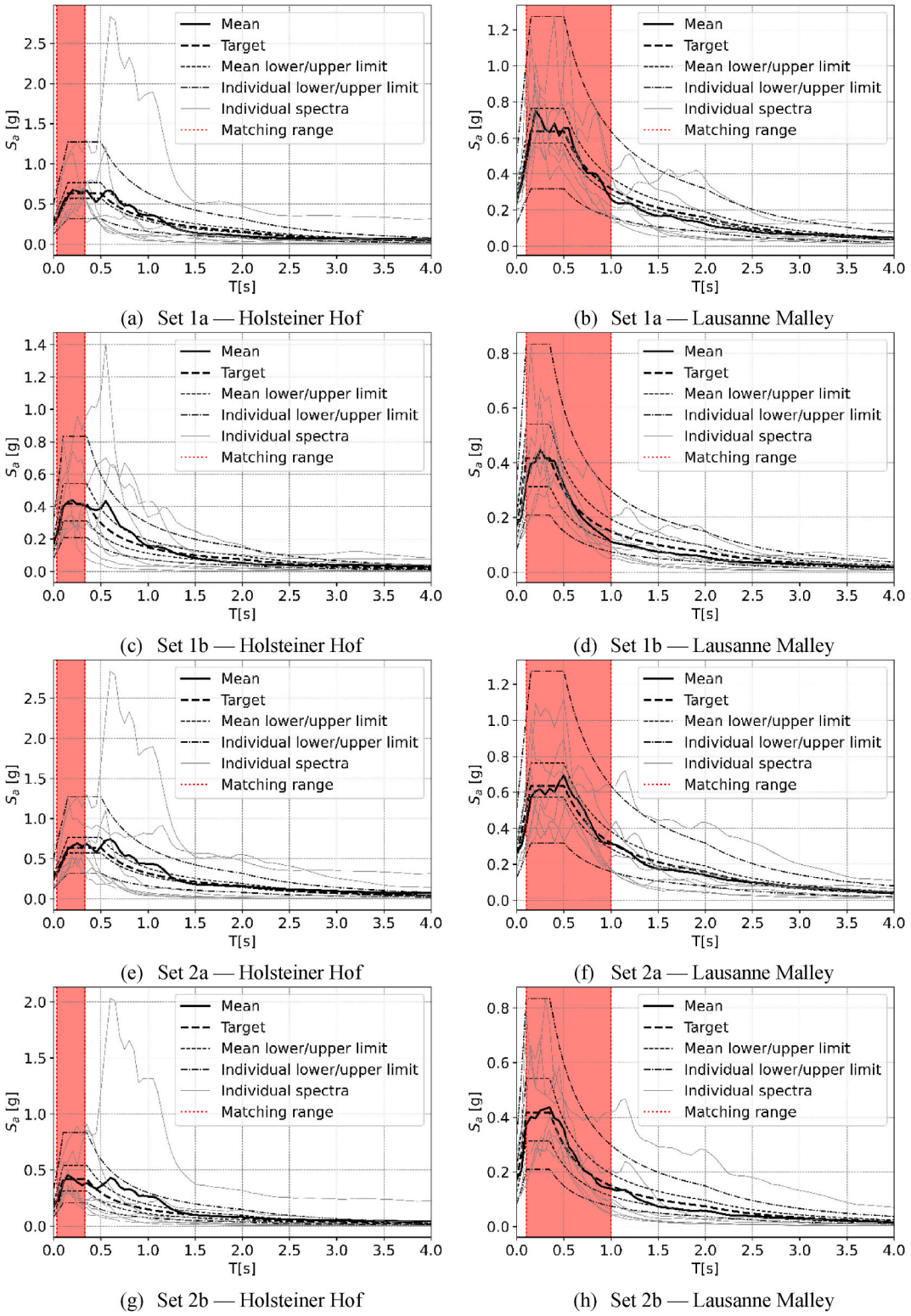


Fig. 5. Sets of records — Soil type B.

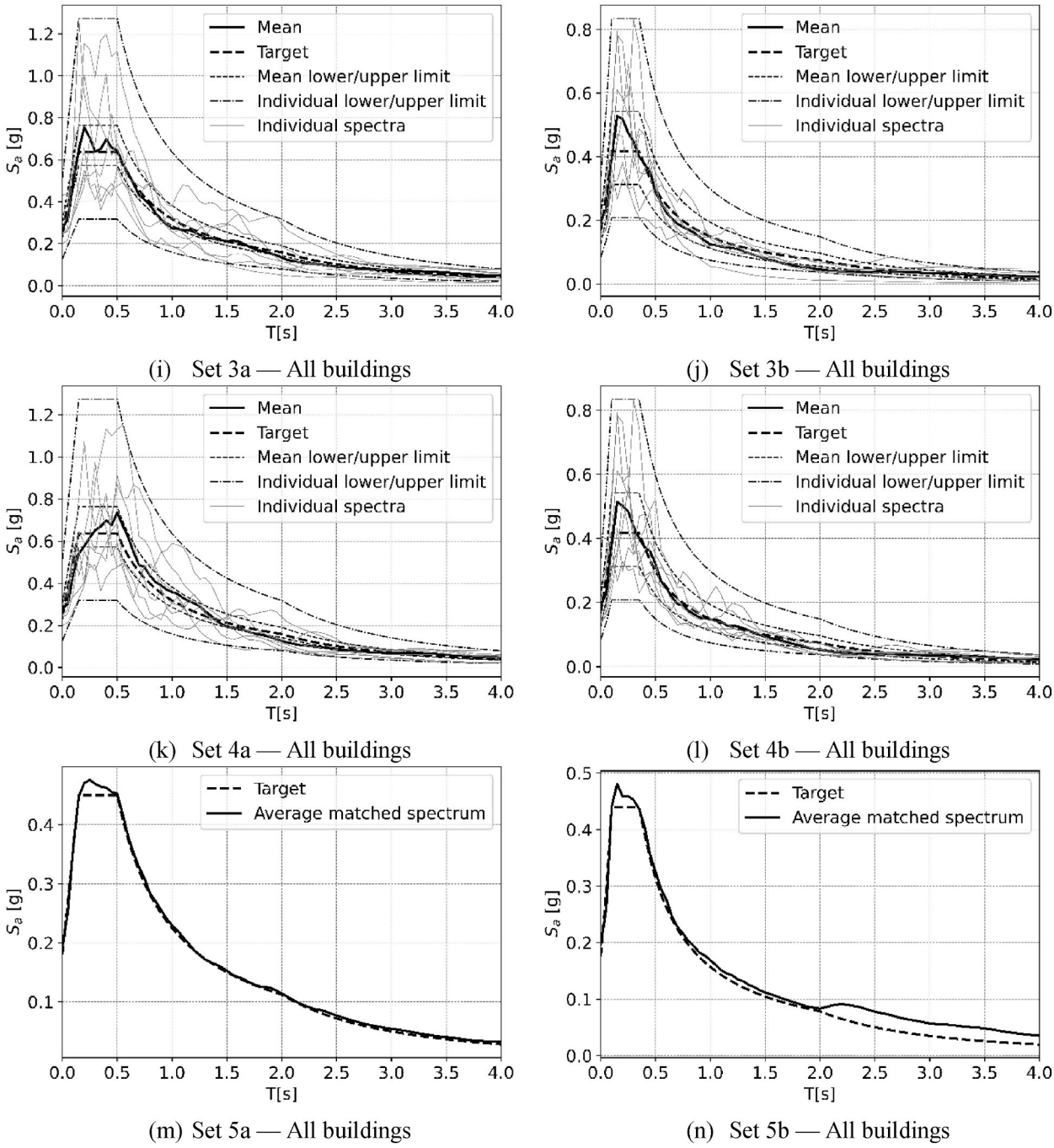


Fig. 5. (*continued*).

This study focuses on bedrock conditions (i.e., soil type A with $V_{S30} \geq 800$ m/s) and further examines the effects of soil amplification by also targeting soil profiles B and C. Regardless of the code version, these profiles are defined by V_{S30} values in the range 360–800 m/s and 180–360 m/s, respectively. Additional seismological conditions are set as $M_w \geq 4.5$, $R_{JB} \geq 15$ km, and no pulse-like records [78]. Figs. 4–6 show the sets of records named according to the definition provided in Table 3 for soil types A, B, and C. The parameters used to derive the target spectra, $a_{gR} = 0.15$g, $S_{\alpha,RP} = 0.35$g, and $S_{\beta,RP} = 0.10$g, were obtained from the maps available in the EFEHR Hazard web platform, based on the latest European Seismic Hazard Model 2020 (ESHM20) [79]. This information corresponds to a site located at coordinates (−8.673, 37.102), which is characterised by moderate to high seismic hazard, as also noted by Macedo and Castro [41]. It should be noted that the utilisation of these parameters leads to the definition of elastic spectra associated with the significant damage (SD) limit state according to Part 3 of Eurocode 8 [46] with a return period of $T_r = 475$ years. The same

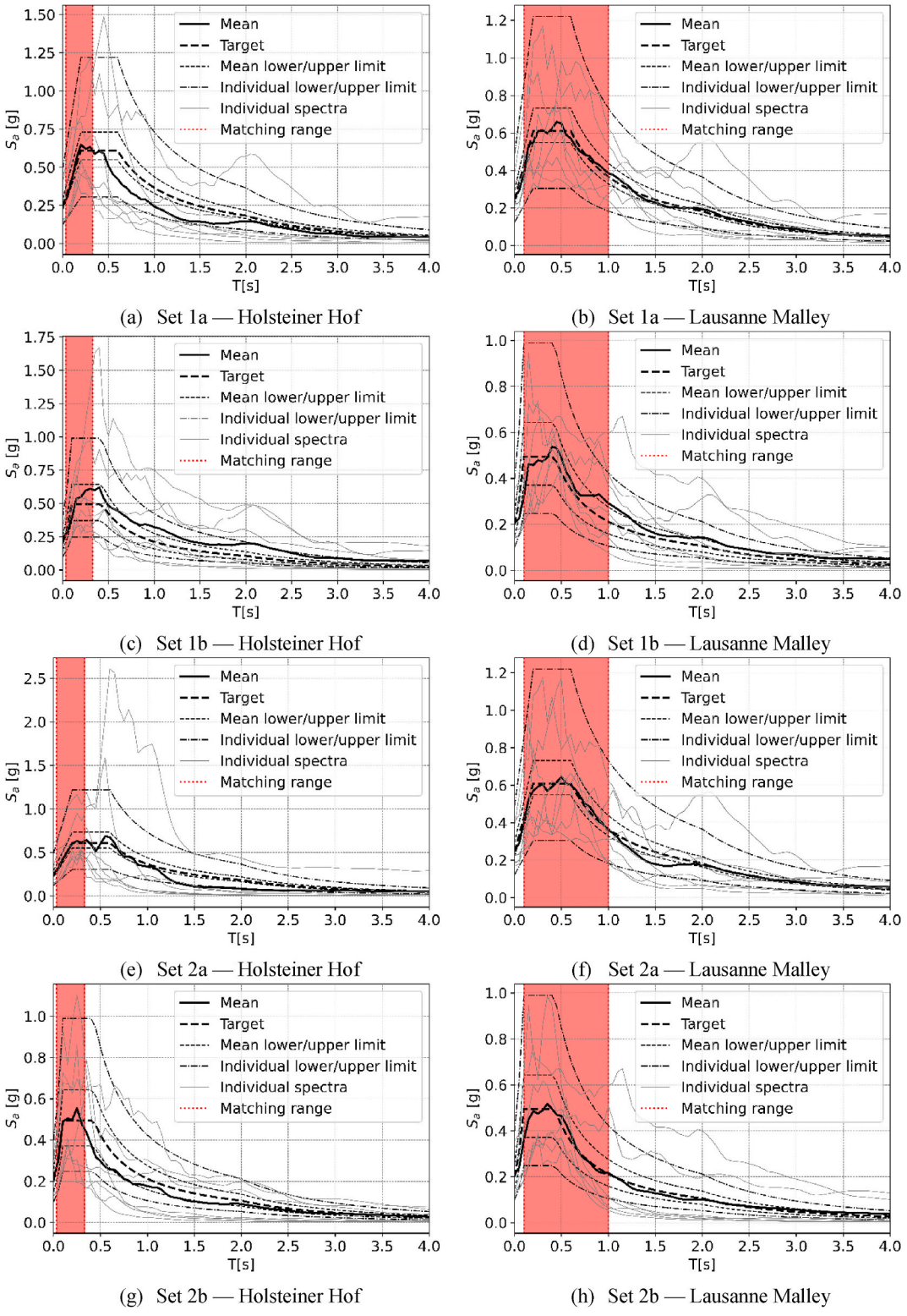


Fig. 6. Sets of records — Soil type C.

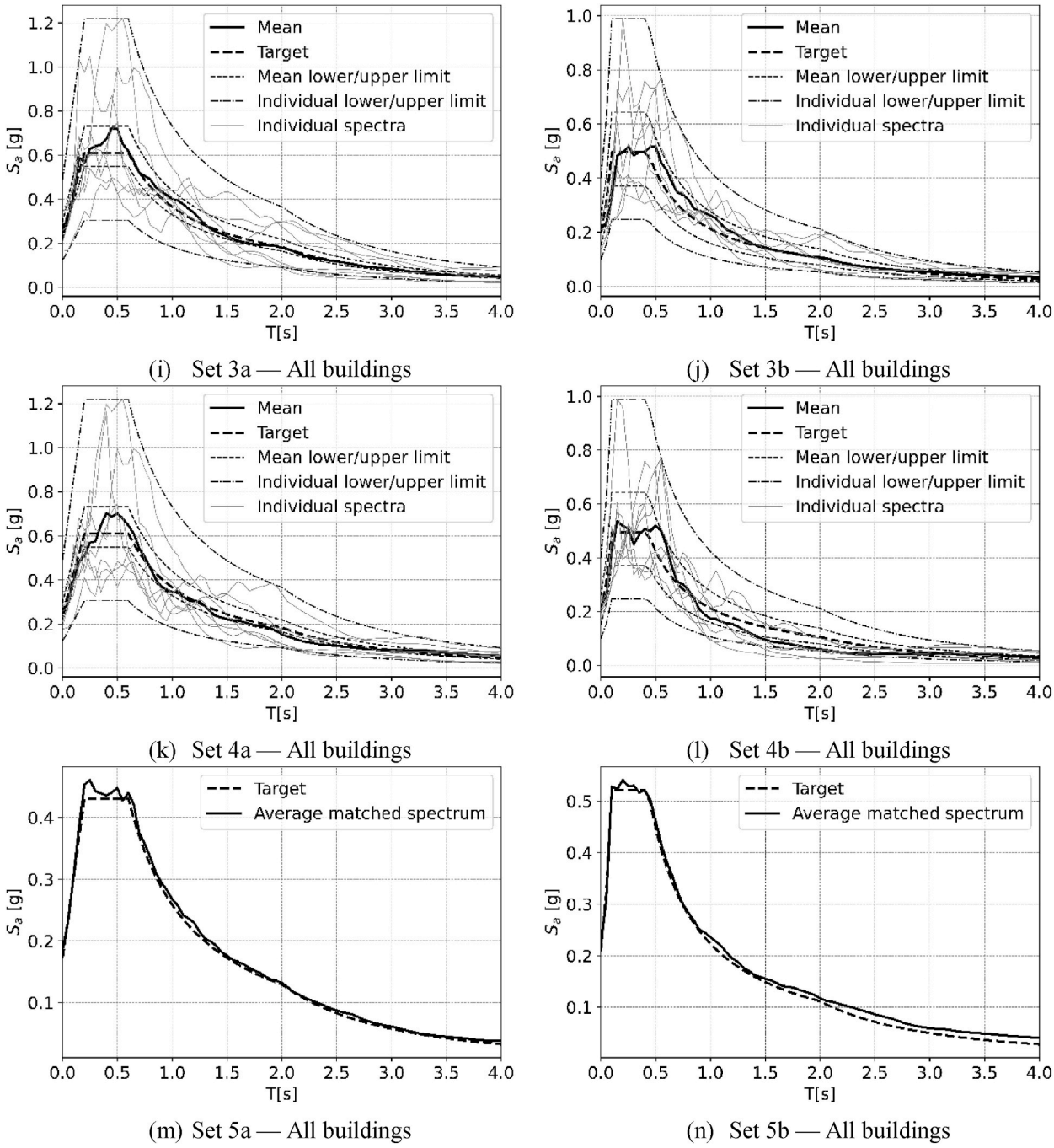


Fig. 6. (*continued*).

Table 4
Summary of target spectrum parameters for both code generations.

EN 1998-1-1:2004		EN 1998-1-1:2024	
Type	1	$S_{\alpha,\mathrm{RP}}$	0.35g
a_{gR}	0.15g	$S_{\beta,\mathrm{RP}}$	0.10g
γ_{I}	1	F_{A}	2.5
$\eta = 1$	1	x	4
–	–	F_{T}	1

target can be linearly scaled to match target spectra at different limit states [40]. Table 4 summarises the target spectrum parameters adopted for reproducing the spectral shape defined in each code generation. Eurocode 8 does not impose the use of the vertical component of seismic action for the case of unreinforced masonry structures [46]. Its consideration is mandatory when the PGA is greater than 0.25g or in specific cases in which the modal response in the vertical direction is relevant to the global behaviour of the structure. Numerical evidence supports that records with predominant near-fault effects (*i.e.*, $R_{JB} < 10$ km) significantly influence both horizontal and vertical seismic demands, particularly in low vibration periods. Since earthquake distances are bounded in the selection process as $R_{JB} \geq 15$ km, the vertical component of seismic action is neglected in this research, which is also supported by some experimental shake-table studies that reported a marginal effect of vertical components on the seismic performance of unreinforced masonry buildings [80]. Nevertheless, a recent study by Di Michele et al. [81] stressed the importance of the vertical component on unreinforced masonry buildings when near-fault records, particularly those from large magnitude ($M_w \geq 6.5$) earthquakes, are considered. Thus, further examination of this aspect is recommended for future research.

The records are selected from a large catalogue, including accelerograms from the reference database for seismic ground motion in Europe (RESORCE) [82], the pan-European engineering strong motion (ESM) [83], the Turkish accelerometric database provided by disaster and emergency management presidency (AFAD) [84], and the Italian accelerometric archive (ITACA) [85]. The same databases have been adopted for earthquake selection to assess the case study buildings, as described in section 2.1, in the context of probabilistic seismic demand analysis (PSDA) [52] and incremental dynamic analysis (IDA) [51].

4. Analysis of results

This section presents a detailed discussion of the results of non-linear time history analyses conducted for the two case study buildings subjected to the action of the ground motion sets presented in section 3. Since both structures are modelled through the equivalent frame model (EFM) approach, the analysis focuses on examining indicators of global behaviour. The idealisation of the structure in piers and spandrels usually leads to the definition of a mechanical system with a limited representation of damage (i.e., less realistic prediction of cracking patterns and local failure mechanisms). Therefore, the maximum average roof displacement, $\max(\overline{\Delta_r})$, and maximum base shear, $\max(V_b)$, are selected as engineering demand parameters (EDPs) for the analysis of the global response. Further investigation on alternative EDPs that can capture local failure mechanisms should be conducted in future work (e.g., residual or peak displacement). The $\max(\overline{\Delta_r})$ is selected as a critical indicator of damage and response in the non-linear range of structural elements. On the other hand, the $\max(V_b)$ represents the strength of the case study building by quantifying the total lateral force resisted at the base after seismic events. This serves as a measure of the overall seismic demand and potential damage to the structure. [63]. The reaction forces at the base nodes are computed at each step of the response history analysis and summed up individually for each direction (i.e., "x" and "y" axes). A resultant force vector is then obtained by calculating the square root of the sum of the squares of these directional components. The $\max(V_b)$ corresponds to the maximum value of the vector previously calculated. For a better representation of inertial properties, the macroelement formulation proposed by Vanin et al. [48], assumes a non-uniform distribution of the element's mass to its three nodes (See Fig. 1a); 2/3 of the mass is assigned to the central node, while the remaining 1/3 portion of the mass is distributed evenly to the bottom and top nodes of the macroelement. The portion of the mass at the bottom nodes of the piers located at the ground level, near the foundation, is not accounted for in the computation of the base shear, as they are assumed to move solidly with the ground [86]. Particularly for the case of low-rise, short-period masonry structures, the $\max(V_b)$ is a good indicator of the record-to-record variability since ground motion sets with considerable PGA variability will lead to higher base shear dispersion. The selection of these global EDPs is in agreement with the analyses presented in Refs. [51,52]. Discussion is presented next separately for each case study building.

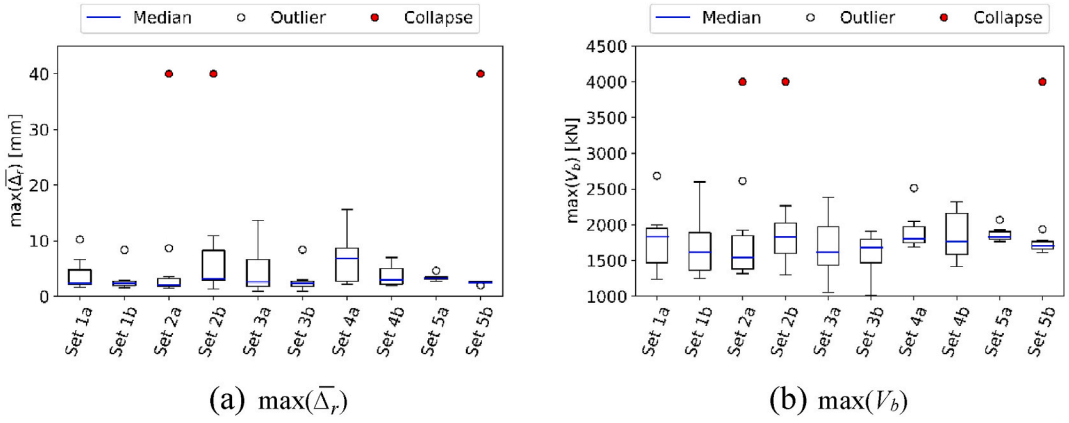


Fig. 7. Box plot Holsteiner Hof — Soil type A.

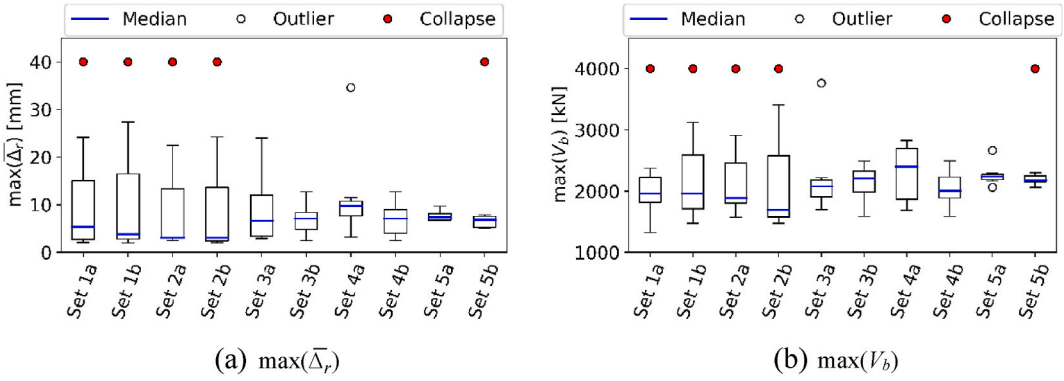


Fig. 8. Box plot Holsteiner Hof — Soil type B.

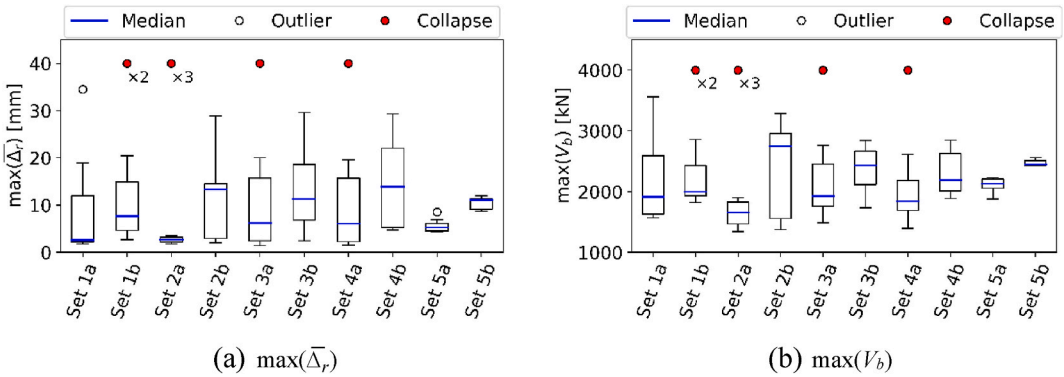


Fig. 9. Box plot Holsteiner Hof — Soil type C.

4.1. Holsteiner Hof

Figs. 7–9 show the numerical results in terms of max($\overline{\Delta_r}$) and max(V_b) for soil types A, B, and C, respectively. Box-whisker diagrams are employed to show the distribution of numerical data for each set of ground motion records. The shape of the box provides a clear representation of the general trend of the data, emphasizing the median values of each ground motion set. The whiskers (the lines extending from the box on both sides) extend to the minimum and maximum data values of EDP. Outliers are identified as the values that fall above or below the ends of the whiskers. Additionally, collapse and non-collapse observations are depicted independently within the plots to show a more consistent statistical representation of the data. It is noted that collapse is identified with a multiplier of record numbers in case more than one collapse is found. As in [52], asymptotic values of 40.00 mm and 4000 kN are set to represent the global collapse in terms of max($\overline{\Delta_r}$) and max(V_b) metrics. These values denote the largest possible non-collapse data, and they are used to bound the collapse damage state.

On bedrock, the median of max($\overline{\Delta_r}$) ranges from 2.07 mm to 6.81 mm for Sets 2a and 4a, respectively (See Fig. 7a). These same sets produce the minimum and maximum base shear forces (max(V_b)), corresponding to 1544 and 1836 kN. Relaxation of constraints in Sets 4a and 4b induces the largest variability in the results of max($\overline{\Delta_r}$) and max(V_b), respectively. On the contrary, and regardless of the EDP, Set 5a and Set 5b drastically reduce the effects of the record-to-record variability in the dynamic response of the building. The extreme values of max($\overline{\Delta_r}$) are 0.91 mm and 15.64 mm, observed in Set 3b and Set 4a. Similarly, the extreme values for the max(V_b), range from 1007 kN (Set 3b) to 2686 kN (Set 1a), followed closely by Sets 2a and 4a. In general, the extreme values of EDPs align with records showing extreme PGA. Except for the three collapse cases in Set 2a, Set 2b, and Set 5b, the Holsteiner Hof building remained mainly elastic after exposure to seismic records. This implies that low-intensity seismic events produce correspondingly low EDP values, while high-intensity records lead to increased EDP observations.

For soil type B, the median of the max($\overline{\Delta_r}$) ranges between 2.84 mm for set 2b and 11.54 mm for Set 4a (See Fig. 8a). The median of max(V_b) in Fig. 8b varies between 1640 kN and 2400 kN, for the same sets, Set 2b and Set 4a, respectively. Further, Set 1b and Set 2b (i.e., US with full and partial consideration of seismological constraints targeting the new shape of the soil B spectrum) lead to the highest dispersion in terms of max($\overline{\Delta_r}$) and max(V_b). The highest number of non-collapse observations occurred in Set 4a and Set 3a, corresponding to max($\overline{\Delta_r}$) = 34.62 mm and max(V_b) = 3763 kN. Likewise, the minimum values are max($\overline{\Delta_r}$) = 1.97 mm and max(V_b) = 1325 kN, both observed in Set 1a. In opposition, the lowest dispersion for both EDPs is achieved by Set 5a (i.e., SM to the old shape of

the soil B spectrum) with median values of max($\overline{\Delta_r}$) = 7.38 mm and max(V_b) = 2240 kN.

The amplification in soil shape C leads to more collapse cases, mainly in Set 2a and Set 1b. The median max($\overline{\Delta_r}$) computed for soil type C varies from 2.64 mm in Set 1a up to 13.94 mm for Set 4b. Similarly, the median value of max(V_b) varies between 1660 kN for Set 1a and 2750 kN for Set 2b. The largest dispersion, or record-to-record variability, is observed within Set 4b and Set 2b for the max($\overline{\Delta_r}$) and max(V_b), respectively. The peak value of max($\overline{\Delta_r}$) corresponds to 29.63 mm, observed in Set 3b, although Set 2b and Set 3b lead to comparable values. Similarly, max(V_b) = 3565 kN is computed within Set 1a. Minimum values of both EDPs are obtained in Set 2a, corresponding to max($\overline{\Delta_r}$) = 1.80 mm, and max(V_b) = 1345 kN. Set 2a also leads to the lowest record-to-record variability in terms of max($\overline{\Delta_r}$), although that distribution corresponds only to 4 non-collapse observations. Instead, when accounting for all seven records, Set 5a provides the smallest dispersion, as in the case of soil type B. In terms of max(V_b), Set 5b (i.e., spectral matching to the soil C spectrum shape) shows the lowest dispersion.

Fig. 10 illustrates the capacity curves of the Holsteiner Hof building in terms of PGA derived from IDA. These curves, presented in [51], were generated using 21 input ground motions from the same database employed in this study to select earthquake record sets for non-linear response history analyses. The results are summarised by the 50th percentile (median), 16th, and 84th quantiles, along with the performance points for Immediate Occupancy (IO) and Collapse Prevention (CP). These curves provide an approximation of the building's "true" mean numerical response. Besides, the acceleration records used in [51] to derive the IDA curves are representative of soil profiles A, B, and C. The values of $a_g S$ (See Fig. 3a) denoting the target PGA in the old shape of the spectrum are 0.15, 0.18, and 0.17 g for soil types A, B, and C, respectively. Analogously, the values of S_α/F_A for the new shape, depicted in Fig. 3b, are 0.14, 0.18, and 0.21 g, for the same soil types, respectively. Subsequently, in the same order, the 50th fractile gives estimations of the median values of max($\overline{\Delta_r}$) as 3.43, 6.24, and 5.54 mm for the old shape and 3.08, 5.83, and 8.89 mm for the new one. For the bedrock case, the closest estimations to the median response, matching the old shape of the target spectrum, are given by Set 3a and Set 5a with relative errors of 33.7 % and 5.62 %, respectively. Sets "b", in general, provided good approximations to the median with a maximum relative error of 23.54 % in Set 1b; this is again attributed to the fact that the structure remained mainly elastic, and its response is proportional to the level of intensity in the signal. For soil type B, the closest approximation to the median is found in Sets 3a and Set 5b regarding the old and new shapes of the code-based spectrum, with relative errors of 5.5 % and 11.7 %, respectively. On the other hand, for soil type C and the previous code-based spectrum, Set 4a provides a close approximation to the median, with a relative error of 3.7 %, followed by Set 3a with a relative error of 6.7 %. For the new shape, the closest estimation of the median is given by Set 1b, emphasizing the importance of seismological constraints in the selection process of input motions whenever possible.

4.2. Lausanne Malley

The results of non-linear time history analyses are consistent with the observations made in Refs. [51,52], where the Lausanne Malley was found to be a highly vulnerable building. A considerable part of the earthquake motions led the building to global collapse regardless of the relatively low-intensity levels in terms of PGA, as depicted in Figs. 4–6. Fig. 11 shows the scatter of EDPs for soil type A. Set 2b and Set 4a provide the lowest and highest estimation of the median values of EDP and as 11.33 mm and 30.61 mm for the max ($\overline{\Delta_r}$), and 3025 and 4068 kN for the max(V_b), respectively. The highest variability in the response is given by Set 3a and Set 3b for the max($\overline{\Delta_r}$) and max(V_b), respectively. In contrast, Set 5a and Set 5b exhibit the lowest dispersion, regardless of the chosen EDP.

As shown in Fig. 12, all motions within Sets 1a, 3b, 4b, and 5a for soil type B led the building to global collapse. Similarly, six out of seven records in Sets 2a, 2b, and 3a induced collapse. The non-collapse observations generated by the remaining recording in Fig. 12 correspond to max($\overline{\Delta_r}$) = 71.01 mm, max(V_b) = 4829 kN; max($\overline{\Delta_r}$) = 20.40 mm, max(V_b) = 3483 kN; and max($\overline{\Delta_r}$) = 55.30 mm, max (V_b) = 4446 kN, for Sets 2a, 2b, and 3a respectively. For Sets 1b, 4a, and 5b, the median EDPs shown in Fig. 12 are max($\overline{\Delta_r}$) = 23.09 mm, max(V_b) = 4050 kN; max($\overline{\Delta_r}$) = 68.40 mm, max(V_b) = 4746 kN; and max($\overline{\Delta_r}$) = 31.55 mm, max(V_b) = 4411 kN; out of which Set 1b and Set 4a induced the largest and lowest record-to-record variability for non-collapse data, respectively. Next, for soil type C (See Fig. 13), only Set 5b showed collapse for all ground motion records. For the other sets, the non-collapse median values of max($\overline{\Delta_r}$) vary from 34.38 mm in Set 1b up to 49.98 mm in Set 4b. Similarly, the median max(V_b) varies between 3872 and 4788 kN. The minimum values of global EDPs correspond to the outlier in Set 2b, with max($\overline{\Delta_r}$) = 27.23 mm, and max(V_b) = 3518 kN. Besides, the lowest

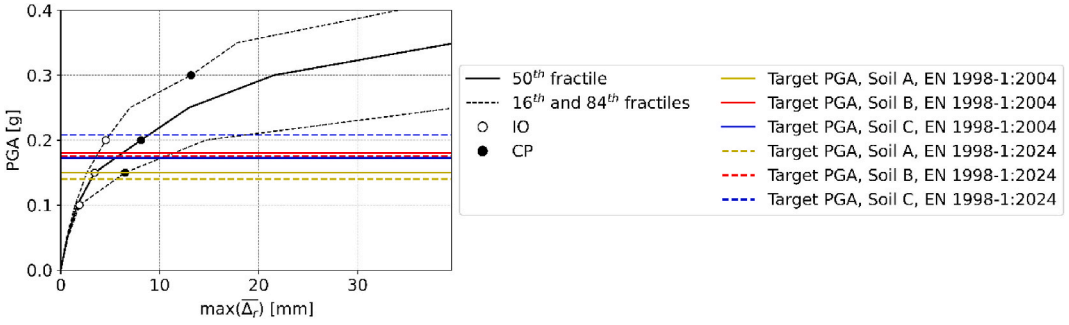


Fig. 10. Capacity curve in terms of PGA — Holsteiner Hof (Caicedo et al. [51]).

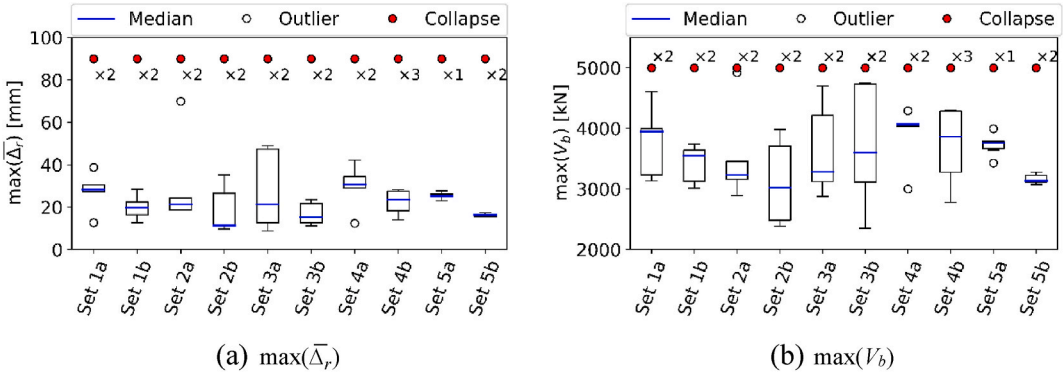


Fig. 11. Box plot Lausanne Malley — Soil type A.

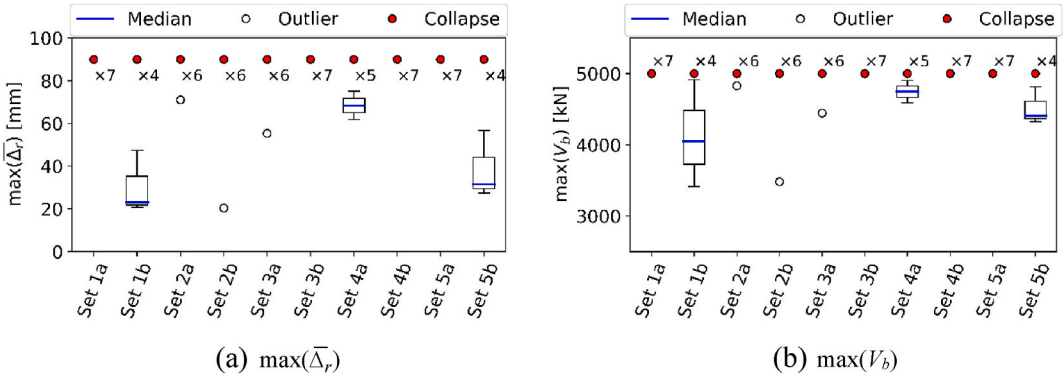


Fig. 12. Box plot Lausanne Malley — Soil type B.

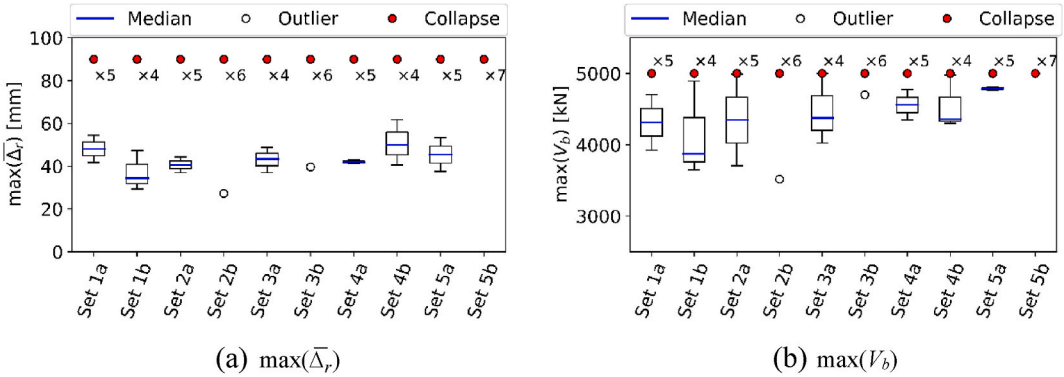


Fig. 13. Box plot Lausanne Malley — Soil type C.

variability is achieved by utilising Set 4a and Set 5a in terms of max($\overline{\Delta_r}$) and max(V_b), respectively. Contrastingly, Set 1b induces the highest dispersion for both global metrics under analysis.

Fig. 14 shows the IDA capacity curves in terms of PGA for the Lausanne Malley, indicating the PGA of each target in the selection. Under EN 1998-1-1:2004 spectrum, the median max($\overline{\Delta_r}$) estimated from the target values of PGA are 31.44 mm, 66.58 mm, and 57.79 mm for soil types A, B, and C, respectively. In comparison, for EN 1998-1-1:2024 spectrum, the values are 28.10 mm for soil A, 61.46 mm for soil B, and greater than 90.00 mm (i.e., global collapse) for soil C. For soil type A, Set 4a and Set 4b deliver the best approximation to the median response by targeting the values of PGA from EN 1998-1-1:2004 and EN 1998-1-1:2024 with relative errors of 2.63 % and 16.20 %, respectively.

For soil type B, the closest estimation of the median demand from a target value of PGA = 0.18 g (EN 1998-1-1:2004) is observed in Set 4a with a relative error of 2.7 % regarding the non-collapse observations. In general, poor estimations are delivered by Sets "b"

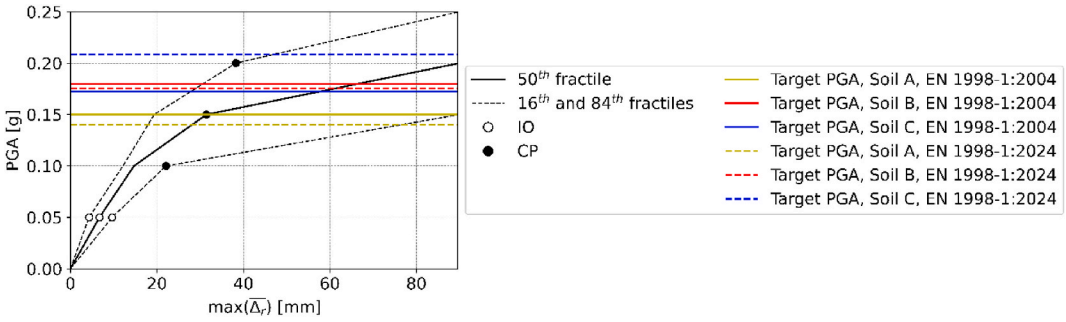


Fig. 14. Capacity curve in terms of PGA — Lausanne Malley (Caicedo et al. [51]).

(targeting the latest spectral shape), particularly for soil type B. In this sense, the closest value to the median is given by Set 5b with a relative error of 48.7 % (See Fig. 12a), indicating that more records are required to improve the accuracy of the estimations. Moving to soil type C, the best approximation to the median value from the old shape of the spectrum is delivered by Set 1a with a 16.8 % relative error, followed closely by Set 5a with a relative error of 21.3 %. Lastly, by targeting the EN 1998-1-1:2024 soil C spectrum, Sets 2b, 3b, and 5b are sufficient to provide reasonable estimations of collapse since the majority of records within the sets induced the global failure of the building.

4.3. Record-to-record variability

In general, for both buildings, the highest record-to-record variability is observed for Set 1b and Set 2b. These sets have in common the matching range $0.2T_1$–$1.5T_1$, while in Set 1a and Set 2a, with a broader matching range, the dispersion is less. This is even more noticeable for Sets "3", "4", and "5", in which, regardless of the code version and constraint conditions, the dispersion decreases drastically when the selection process targets the spectra in the broader range. This is attributed to the participation of higher modes in the dynamic response as well as the elongation of the fundamental period, T_1, as a clear indicator of structural inelasticity because of damage accumulation. Thus, one important limitation of code-based selection approaches seems to be the narrow matching ranges, in terms of T_1, defined in the standards, e.g., 0.2 T_1–2.0 T_1 in the former EN 1998 and 0.2 T_1–1.5 T_1 in the later revision. Shaking table tests conducted on various examples of unreinforced masonry structures with flexible diaphragms support this claim. In these experiments, the first-mode period progressively elongated up to twice the undamaged fundamental period [86,87] or even 3.5 times of the undamaged T_1 in the worst-case scenario [88]. Another factor that can be attributed to the reduction in dispersion, when matching a broader period range, is the contribution of higher modes and activation of potential OOP failure mechanisms due to earthquake excitations [89,90]. The advanced macroelement approach implemented in this research allows for the consideration of OOP local failure modes that, otherwise, would be impossible to consider with conventional macroelement approaches [91,92]. Previous applications of the three-dimensional macroelement showed how earthquake loads induced OOP failures (i.e., partial or total overturning of the façade), corresponding to OOP local modes that can occur at lower frequencies [49,52]. On the other hand, although dispersion decreases within Sets "3", "4", and "5", they also lead to higher estimations of the median, which suggests that targeting the elastic response spectrum shape, either EN 1998-1-1:2004 or EN 1998-1-1:2024, is a rather conservative approach. Alternative targets, such as UHS and CMS, are likely to provide more realistic estimations of the median response as suggested in Refs. [93,94]. Generally, the closest approximation of the median response, derived from capacity curves, was achieved by datasets that incorporated seismological constraints during the preselection phase. This observation aligns with the findings of previous studies [33,40] since complying with the specific seismological and geological conditions will ensure spectral compatibility with hazard-consistent scenarios. The spectral shape is intrinsically influenced by seismological parameters, such as magnitude and distance (M, R) pairs [15], which are key parameters in more refined selection methodologies like those employed in Refs. [51,52]. Finally, it is worth noting that all analysed sets consist of seven acceleration records, which, in some cases, could not reach a satisfactory compatibility with the median demand estimated from IDA capacity curves. That is the case of EN 1998-1-1:2024 soil type B, where the best approximation resulted in a relative error approaching 50 %. These results imply the need to revise and validate the number of accelerograms required for a reliable estimation of the '*true*' mean seismic demand using probabilistic methods, specifically for pre-code unreinforced masonry constructions, where record-to-record variability plays a critical role.

5. Conclusions

The seismic safety of old masonry buildings under bi-directional earthquake loads was addressed in this paper. Detailed three-dimensional models of two buildings were developed in OpenSees, accounting for in-plane (IP) and out-of-plane (OOP) masonry wall effects, as well as non-linear wall and floor connections. Input motion targets were based on spectral shapes from EN 1998-1-1:2004 and EN 1998-1-1:2024, using a 475-year return period. A metaheuristic algorithm selected ten accelerogram suites, reflecting differences in Eurocode versions, seismological constraints, period-domain matching, and scaling strategies. Besides soil profile A, soil amplification effects were analysed for soil profiles B and C. Non-linear response history analyses were conducted to examine the

variability in structural response stemming from record-to-record uncertainty.

Based on the numerical findings of this research, the following observations are valid for the code-based selection of earthquake motions for seismic evaluation of short-period old masonry buildings:

- Whenever possible, seismological constraints should be accounted for in the preselection process of input motions to deliver a more realistic approximation of the seismic demand.
- Aimed at reducing the dispersion of the seismic response, the matching strategy should fit the target spectrum in a broader matching range (*i.e.*, 0.0 s $\leq T \leq$ 4.0 s) and not just a range defined around the fundamental elastic period, T_1, since higher modes and period lengthening because of cumulative damage play a relevant role in the dynamic behaviour of pre-code masonry constructions.
- Targeting the elastic design spectrum defined in either the EN 1998-1-1:2004 or the EN 1998-1-1:2024 editions of Eurocode 8 resulted in higher estimations of the median response, showing better accuracy when the spectral shape from the first-generation code edition was selected as the target. The effect of alternative, less conservative targets, such as the uniform hazard spectrum or conditional mean spectrum, on the seismic demand of unreinforced masonry buildings is encouraged to be examined in future research.

Finally, the median response in terms of global EDPs may exhibit significant relative errors, reaching up to 50 % in the worst-case scenario (as shown for soil type B, EN 1998-1-1:2024). This underscores the need to revise and validate the minimum number of records required for a reliable estimation of the '*true*' mean seismic demand from a probabilistic perspective, specifically, for the case of pre-code masonry constructions, in which record-to-record variability significantly influences the outcomes. Future work should focus on the application of probabilistic methods on representative masonry archetypes, considering the mixed effect of record-to-record variability and quantification of model uncertainty (e.g., variation in mechanical properties), to provide complementary guidance for selecting earthquake ground motions, which is often based on engineering experience.

CRediT authorship contribution statement

Daniel Caicedo: Writing – original draft, Visualization, Validation, Software, Methodology, Investigation, Formal analysis, Conceptualization. **Igor Tomić:** Writing – review & editing, Visualization, Validation, Supervision, Software, Methodology, Investigation, Formal analysis, Conceptualization. **Shaghayegh Karimzadeh:** Writing – review & editing, Visualization, Validation, Resources, Methodology, Investigation, Conceptualization. **Vasco Bernardo:** Writing – review & editing, Visualization, Supervision, Methodology, Conceptualization. **Katrin Beyer:** Writing – review & editing, Visualization, Supervision, Resources, Project administration, Conceptualization. **Paulo B. Lourenço:** Writing – review & editing, Validation, Supervision, Resources, Project administration, Funding acquisition, Conceptualization.

Declaration of competing interest

The authors declare that they have no known competing financial interests or personal relationships that could have appeared to influence the work reported in this paper.

Acknowledgment

This study has been partly funded by the STAND4HERITAGE project that has received funding from the European Research Council (ERC) under the European Union's Horizon 2020 research and innovation program (Grant agreement No. 833123), as an Advanced Grant. This work was also partly financed by FCT/MCTES through national funds (PIDDAC) under the R&D Unit Institute for Sustainability and Innovation in Structural Engineering (ISISE), under reference UIDB/04029/2020 (doi.org/10.54499/UIDB/04029/2020), and under the Associate Laboratory Advanced Production and Intelligent Systems ARISE under reference LA/P/0112/2020. This work is partly financed by national funds through FCT - Foundation for Science and Technology, under grant agreement 2023.01101.BD attributed to the first author. The second author was supported by the Swiss National Science Foundation through grant 200021_175903/1 Equivalent frame models for the in-plane and OOP response of unreinforced masonry buildings.

Data availability

The Python scripts for code-based ground motion selection and sets of motions used in this study are shared openly through the repository https://zenodo.org/records/15459442.

References

[1] M. Como, Statics of historic masonry constructions: an essay. Masonry Structures: Between Mechanics and Architecture, 2015, https://doi.org/10.1007/978-3-319-13003-3_3.

[2] L. Danciu, D. Giardini, G. Weatherill, R. Basili, S. Nandan, A. Rovida, et al., The 2020 European Seismic Hazard Model: Overview and Results, vol 2024, EGUsphere, 2024, pp. 1–36.

[3] F. Parisi, N. Augenti, Seismic capacity of irregular unreinforced masonry walls with openings, Earthq. Eng. Struct. Dynam. 42 (2013), https://doi.org/10.1002/eqe.2195.
[4] M. Betti, L. Galano, A. Vignoli, Comparative analysis on the seismic behaviour of unreinforced masonry buildings with flexible diaphragms, Eng. Struct. 61 (2014), https://doi.org/10.1016/j.engstruct.2013.12.038.
[5] Y. Nakamura, H. Derakhshan, G. Magenes, M.C. Griffith, Influence of diaphragm flexibility on seismic response of unreinforced masonry buildings, J. Earthq. Eng. 21 (2017) 935–960, https://doi.org/10.1080/13632469.2016.1190799.
[6] R. Scotta, D. Trutalli, L. Marchi, L. Pozza, Seismic performance of URM buildings with in-plane non-stiffened and stiffened timber floors, Eng. Struct. 167 (2018), https://doi.org/10.1016/j.engstruct.2018.02.060.
[7] I. Tomić, F. Vanin, K. Beyer, Uncertainties in the seismic assessment of historical masonry buildings, Appl. Sci. 11 (2021) 2280.
[8] M. Dolsek, Incremental dynamic analysis with consideration of modeling uncertainties, Earthq. Eng. Struct. Dynam. 38 (2009), https://doi.org/10.1002/eqe.869.
[9] N. Shome, C.A. Cornell, P. Bazzurro, J.E. Carballo, Earthquakes, records, and nonlinear responses, Earthq. Spectra 14 (1998) 469–500.
[10] I. Iervolino, C.A. Cornell, Record selection for nonlinear seismic analysis of structures, Earthq. Spectra 21 (2005), https://doi.org/10.1193/1.1990199.
[11] D. Caicedo, S. Karimzadeh, V. Bernardo, P.B. Lourenço, Selection and scaling approaches of earthquake time-series for structural engineering applications: a rt review, Arch. Comput. Methods Eng. (2023), https://doi.org/10.1007/s11831-023-10025-y.
[12] E.I. Katsanos, A.G. Sextos, G.D. Manolis, Selection of earthquake ground motion records: a state-of-the-art review from a structural engineering perspective, Soil Dynam. Earthq. Eng. 30 (2010), https://doi.org/10.1016/j.soildyn.2009.10.005.
[13] R.K. McGuire, Probabilistic seismic hazard analysis: early history, Earthq. Eng. Struct. Dynam. 37 (2008), https://doi.org/10.1002/eqe.765.
[14] J.W. Baker, An Introduction to Probabilistic Seismic Hazard Analysis (PSHA), 2008.
[15] J.W. Baker, C.A. Cornell, Spectral shape, epsilon and record selection, Earthq. Eng. Struct. Dynam. 35 (2006), https://doi.org/10.1002/eqe.571.
[16] J.W. Baker, Conditional mean spectrum: tool for ground-motion selection, J. Struct. Eng. 137 (2011), https://doi.org/10.1061/(asce)st.1943-541x.0000215.
[17] Y.-N. Huang, A.S. Whittaker, N. Luco, R.O. Hamburger, Scaling earthquake ground motions for performance-based assessment of buildings, J. Struct. Eng. 137 (2011), https://doi.org/10.1061/(asce)st.1943-541x.0000155.
[18] B.Ö. Ay, S. Akkar, Evaluation of a recently proposed record selection and scaling procedure for low-rise to mid-rise reinforced concrete buildings and its use for probabilistic risk assessment studies, Earthq. Eng. Struct. Dynam. 43 (2014), https://doi.org/10.1002/eqe.2378.
[19] A.K. Kazantzi, D. Vamvatsikos, Intensity measure selection for vulnerability studies of building classes, Earthq. Eng. Struct. Dynam. 44 (2015), https://doi.org/10.1002/eqe.2603.
[20] Z. Bayati, M. Soltani, Ground motion selection and scaling for seismic design of RC frames against collapse, Earthq. Struct 11 (2016), https://doi.org/10.12989/eas.2016.11.3.445.
[21] M.A. Hariri-Ardebili, V.E. Saouma, Probabilistic seismic demand model and optimal intensity measure for concrete dams, Struct. Saf. 59 (2016) 67–85.
[22] C. Li, C. Zhai, S. Kunnath, D. Ji, Methodology for selection of the Most damaging ground motions for nuclear power plant structures, Soil Dynam. Earthq. Eng. 116 (2019) 345–357, https://doi.org/10.1016/j.soildyn.2018.09.039.
[23] S. Karimzadeh, K. Kadas, A. Askan, A. Yakut, Comparison of real and simulated records using ground motion intensity measures, Soil Dynam. Earthq. Eng. 147 (2021), https://doi.org/10.1016/j.soildyn.2021.106796.
[24] S. Karimzadeh, K. Kadasa, A. Askanb, M.A. Erberikb, A. Yakutb, Derivation of analytical fragility curves using SDOF models of masonry structures in Erzincan (turkey), Earthq. Struct 18 (2020), https://doi.org/10.12989/eas.2020.18.2.249.
[25] M. Causse, A. Laurendeau, M. Perrault, J. Douglas, L.F. Bonilla, P. Guéguen, Eurocode 8-compatible synthetic time-series as input to dynamic analysis, Bull. Earthq. Eng. 12 (2014), https://doi.org/10.1007/s10518-013-9544-2.
[26] K. Zhong, T. Lin, G.G. Deierlein, R.W. Graves, F. Silva, N. Luco, Tall building performance-based seismic design using SCEC broadband platform site-specific ground motion simulations, Earthq. Eng. Struct. Dynam. 50 (2021), https://doi.org/10.1002/eqe.3364.
[27] J. Fayaz, M. Dabaghi, F. Zareian, Utilization of site-based simulated ground motions for hazard-targeted seismic demand estimation: application for ordinary bridges in southern California, J. Bridge Eng. 25 (2020), https://doi.org/10.1061/(asce)be.1943-5592.0001634.
[28] S. Karimzadeh, M.F. Funari, S. Szabó, S.M.S. Hussaini, S. Rezaeian, P.B. Lourenço, Stochastic simulation of earthquake ground motions for the seismic assessment of monumental masonry structures: source-based vs site-based approaches, Earthq. Eng. Struct. Dynam. (2023), https://doi.org/10.1002/eqe.4012.
[29] P. Code, Eurocode 8: Design of Structures for Earthquake resistance-part 1: General Rules, Seismic Actions and Rules for Buildings, European Committee for Standardization, Brussels, 2005.
[30] Engineers AS of C, Seismic evaluation and retrofit of existing buildings, American Soc. Civil. Eng (2014).
[31] AS. of C. Engineers, Minimum design loads and associated criteria for buildings and other structures, American Soc. Civil. Eng (2017).
[32] N.Z.S. Nzs, Structural design actions part 5: earthquake actions-New zealand, Nzs 1170 (2004) 2004.
[33] A.G. Sextos, E.I. Katsanos, G.D. Manolis, EC8-based earthquake record selection procedure evaluation: validation study based on observed damage of an irregular R/C building, Soil Dynam. Earthq. Eng. 31 (2011), https://doi.org/10.1016/j.soildyn.2010.10.009.
[34] S. Koboevic, K. Guilini-Charrette, P.X. Castonguay, R. Tremblay, Selection and scaling of NBCC 2005 compatible simulated ground motions for nonlinear seismic analysis of low-rise steel building structures, Can. J. Civ. Eng. 38 (2011), https://doi.org/10.1139/L11-094.
[35] NRCC, National Building Code of Canada 2005, twelfth ed., National Research Council of Canada, Ottawa, Ont, 2005, p. n.d..
[36] G.M. Atkinson, Earthquake time histories compatible with the 2005 national building code of Canada uniform hazard spectrum, Can. J. Civ. Eng. 36 (2009), https://doi.org/10.1139/L09-044.
[37] L. Lin, N. Naumoski, M. Saatcioglu, S. Foo, E. Booth, Y. Gao, Selection of seismic excitations for nonlinear analysis of reinforced concrete frame buildings1, Can. J. Civ. Eng. 40 (2013), https://doi.org/10.1139/l2012-103.
[38] D. Michaud, P. Léger, Ground motions selection and scaling for nonlinear dynamic analysis of structures located in eastern North America, Can. J. Civ. Eng. 41 (2014), https://doi.org/10.1139/cjce-2012-0339.
[39] M. Ergun, S. Ates, Selecting and scaling ground motion time histories according to eurocode 8 and ASCE 7-05, Earthq. Struct 5 (2013), https://doi.org/10.12989/eas.2013.5.2.129.
[40] M. Araújo, L. Macedo, M. Marques, J.M. Castro, Code-based record selection methods for seismic performance assessment of buildings, Earthq. Eng. Struct. Dynam. 45 (2016), https://doi.org/10.1002/eqe.2620.
[41] L. Macedo, J.M. Castro, SelEQ: an advanced ground motion record selection and scaling framework, Adv. Eng. Software 114 (2017), https://doi.org/10.1016/j.advengsoft.2017.05.005.
[42] A.H. Kayhan, A. Demir, M. Palanci, Multi-functional solution model for spectrum compatible ground motion record selection using stochastic harmony search algorithm, Bull. Earthq. Eng. 20 (2022) 6407–6440, https://doi.org/10.1007/s10518-022-01450-8.
[43] J.C. Reyes, C. González, E. Kalkan, Improved ASCE/SEI 7-10 ground-motion scaling procedure for nonlinear analysis of buildings, J. Earthq. Eng. 25 (2021), https://doi.org/10.1080/13632469.2018.1526140.
[44] S. Karimzadeh, S.M.S. Hussaini, M.F. Funari, P.B. Lourenço, On the effect of different code-based ground motion selection approaches for the estimation of the seismic demand of masonry structures by using real ground motion, Data Set (2021).
[45] F. Jalayer, H. Ebrahimian, A. Miano, Record-to-record variability and code-compatible seismic safety-checking with limited number of records, Bull. Earthq. Eng. 19 (2021), https://doi.org/10.1007/s10518-020-01024-6.
[46] Code P, Eurocode 8: Design of Structures for Earthquake resistance—Part 3: Assessment and Retrofitting of Buildings, March 2010. Incorporating Corrigendum.
[47] F. McKenna, OpenSees: a framework for earthquake engineering simulation, Comput. Sci. Eng. 13 (2011) 58–66.
[48] F. Vanin, A. Penna, K. Beyer, A three-dimensional macroelement for modelling the in-plane and out-of-plane response of masonry walls, Earthq. Eng. Struct. Dynam. 49 (2020), https://doi.org/10.1002/eqe.3277.

[49] F. Vanin, A. Penna, K. Beyer, Equivalent-frame modeling of two shaking table tests of masonry buildings accounting for their out-of-plane response, Frontiers in Built Environ 6 (2020), https://doi.org/10.3389/fbuil.2020.00042.
[50] M. Valente, Seismic vulnerability assessment and earthquake response of slender historical masonry bell towers in south-east lombardia, Eng. Fail. Anal. 129 (2021), https://doi.org/10.1016/j.engfailanal.2021.105656.
[51] D. Caicedo, I. Tomić, S. Karimzadeh, V. Bernardo, K. Beyer, P.B. Lourenço, Collapse fragility analysis of historical masonry buildings considering in-plane and out-of-plane response of masonry walls, Eng. Struct. 319 (2024) 118804.
[52] D. Caicedo, I. Tomić, S. Karimzadeh, V. Bernardo, K. Beyer, P.B. Lourenço, Optimal intensity measure and probabilistic seismic demand model for the assessment of historical masonry buildings: application to two case studies, Reliab. Eng. Syst. Saf. (2025) 111149.
[53] C. Michel, A. Karbassi, P. Lestuzzi, Evaluation of the seismic retrofitting of an unreinforced masonry building using numerical modeling and ambient vibration measurements, Eng. Struct. 158 (2018) 124–135.
[54] E. Quagliarini, G. Maracchini, F. Clementi, Uses and limits of the equivalent frame model on existing unreinforced masonry buildings for assessing their seismic risk: a review, J. Build. Eng. 10 (2017) 166–182.
[55] A.M. D'Altri, V. Sarhosis, G. Milani, J. Rots, S. Cattari, S. Lagomarsino, et al., Modeling strategies for the computational analysis of unreinforced masonry structures: review and classification, Arch. Comput. Methods Eng. 27 (2020), https://doi.org/10.1007/s11831-019-09351-x.
[56] F. Vanin, D. Zaganelli, A. Penna, K. Beyer, Estimates for the stiffness, strength and drift capacity of stone masonry walls based on 123 quasi-static cyclic tests reported in the literature, Bull. Earthq. Eng. 15 (2017), https://doi.org/10.1007/s10518-017-0188-5.
[57] F. Vanin, K. Beyer, Equivalent Damping Ratio for a Macroelement Modelling the out-of-plane Response of Masonry Walls, 2023.
[58] G.W. Housner, The behavior of inverted pendulum structures during earthquakes, Bull. Seismol. Soc. Am. 53 (1963) 403–417.
[59] N. Hoveidae, A. Fathi, S. Karimzadeh, Seismic damage assessment of a historic masonry building under simulated scenario earthquakes: a case study for arge-tabriz, Soil Dynam. Earthq. Eng. 147 (2021), https://doi.org/10.1016/j.soildyn.2021.106732.
[60] A. Formisano, G. Di Lorenzo, L. Krstevska, R. Landolfo, Fem model calibration of experimental environmental vibration tests on two churches hit by l'Aquila earthquake, Int. J. Architect. Herit. 15 (2021), https://doi.org/10.1080/15583058.2020.1719233.
[61] G. Guerrini, I. Senaldi, S. Scherini, S. Morganti, G. Magenes, Material characterization for the shaking-table test of the scaled prototype of a stone masonry building aggregate. Material Characterization for the Shaking-Table Test of the Scaled Prototype of a Stone Masonry Building Aggregate, 2017, pp. 105–115.
[62] I. Senaldi, G. Guerrini, S. Scherini, S. Morganti, G. Magenes, K. Beyer, et al., Natural stone masonry characterization for the shaking-table test of a scaled building specimen, Proce. Int. Masonry Soc. Conf. 0 (2018).
[63] G. Guerrini, I. Senaldi, F. Graziotti, G. Magenes, K. Beyer, A. Penna, Shake-table test of a strengthened stone masonry building aggregate with flexible diaphragms, Int. J. Architect. Herit. 13 (2019), https://doi.org/10.1080/15583058.2019.1635661.
[64] P.E. Mergos, A.G. Sextos, Selection of earthquake ground motions for multiple objectives using genetic algorithms, Eng. Struct. 187 (2019), https://doi.org/10.1016/j.engstruct.2019.02.067.
[65] A. Kaveh, R.M. Moghanni, S.M. Javadi, Ground motion record selection using multi-objective optimization algorithms: a comparative study, Period. Polytech. Civ. Eng. 63 (2019), https://doi.org/10.3311/PPci.14354.
[66] M. Georgioudakis, M. Fragiadakis, Selection and scaling of ground motions using multicriteria optimization, J. Struct. Eng. 146 (2020), https://doi.org/10.1061/(asce)st.1943-541x.0002811.
[67] L. Moschen, R.A. Medina, C. Adam, A ground motion record selection approach based on multiobjective optimization, J. Earthq. Eng. 23 (2019), https://doi.org/10.1080/13632469.2017.1342302.
[68] S. Yaghmaei-Sabegh, S. Karami, M. Hosseini-Moghadam, Selection and scaling of spectrum-compatible ground motion records using hybrid coded genetic algorithms, Sci. Iran. 24 (2017), https://doi.org/10.24200/sci.2017.4075.
[69] K. Ye, Z. Chen, H. Zhu, Proposed strategy for the application of the modified harmony search algorithm to code-based selection and scaling of ground motions, J. Comput. Civ. Eng. 28 (2014), https://doi.org/10.1061/(asce)cp.1943-5487.0000261.
[70] M. Shahrouzi, M. Sazjini, Refined harmony search for optimal scaling and selection of accelerograms, Sci. Iran. 19 (2012), https://doi.org/10.1016/j.scient.2012.02.002.
[71] A. Haydar Kayhan, K. Armagan Korkmaz, A. Irfanoglu, Selecting and scaling real ground motion records using harmony search algorithm, Soil Dynam. Earthq. Eng. 31 (2011), https://doi.org/10.1016/j.soildyn.2011.02.009.
[72] I. Iervolino, C. Galasso, R. Paolucci, F. Pacor, Engineering ground motion record selection in the ITalian ACcelerometric archive, Bull. Earthq. Eng. 9 (2011), https://doi.org/10.1007/s10518-011-9300-4.
[73] I. Iervolino, C. Galasso, E. Cosenza, REXEL: computer aided record selection for code-based seismic structural analysis, Bull. Earthq. Eng. 8 (2010), https://doi.org/10.1007/s10518-009-9146-1.
[74] R. Storn, K. Price, Differential evolution - a simple and efficient heuristic for global optimization over continuous spaces, J. Global Optim. (1997), https://doi.org/10.1023/A:1008202821328.
[75] D. Caicedo, L. Lara-Valencia, J. Blandon, C. Graciano, Seismic response of high-rise buildings through metaheuristic-based optimization using tuned mass dampers and tuned mass dampers inerter, J. Build. Eng. 34 (2021), https://doi.org/10.1016/j.jobe.2020.101927.
[76] N.A. Abrahamson, Non-stationary spectral matching, Seismol Res. Lett. 63 (1992) 30.
[77] J. Hancock, J. Watson-Lamprey, N.A. Abrahamson, J.J. Bommer, A. Markatis, E.M.M.A. McCoy, et al., An improved method of matching response spectra of recorded earthquake ground motion using wavelets, J. Earthq. Eng. 10 (2006), https://doi.org/10.1080/13632460609350629.
[78] S.K. Shahi, J.W. Baker, An efficient algorithm to identify strong-velocity pulses in multicomponent ground motions, Bull. Seismol. Soc. Am. 104 (2014) 2456–2466.
[79] L. Danciu, S. Nandan, C. Reyes, R. Basili, G. Weatherill, C. Beauval, et al., The 2020 update of the european seismic hazard model: Model overview, EFEHR Techn. Rep 001 (2021) v1. 0.0.
[80] S. Kallioras, F. Graziotti, A. Penna, G. Magenes, Effects of vertical ground motions on the dynamic response of URM structures: comparative shake-table tests, Earthq. Eng. Struct. Dynam. 51 (2022), https://doi.org/10.1002/eqe.3569.
[81] F. Di Michele, C. Cantagallo, E. Spacone, Effects of the vertical seismic component on seismic performance of an unreinforced masonry structures, Bull. Earthq. Eng. 18 (2020), https://doi.org/10.1007/s10518-019-00765-3.
[82] S. Akkar, M.A. Sandıkkaya, M. Şenyurt, A.A. Sisi, B. Ay, P. Traversa, et al., Reference database for seismic ground-motion in europe (RESORCE), Bull. Earthq. Eng. 12 (2014), https://doi.org/10.1007/s10518-013-9506-8.
[83] G. Lanzano, S. Sgobba, L. Luzi, R. Puglia, F. Pacor, C. Felicetta, et al., The pan-European engineering strong motion (ESM) flatfile: compilation criteria and data statistics, Bull. Earthq. Eng. 17 (2019) 561–582.
[84] Disaster, Authority EM, Turkish national strong motion network. https://doi.org/10.7914/SN/TK, 1973.
[85] L. Luzi, S. Hailemikael, D. Bindi, F. Pacor, F. Mele, F. Sabetta, ITACA (ITalian ACcelerometric archive): a web portal for the dissemination of the Italian strong motion data, Seismol Res. Lett. (2008).
[86] S. Kallioras, G. Guerrini, U. Tomassetti, B. Marchesi, A. Penna, F. Graziotti, et al., Experimental seismic performance of a full-scale unreinforced clay-masonry building with flexible timber diaphragms, Eng. Struct. 161 (2018), https://doi.org/10.1016/j.engstruct.2018.02.016.
[87] S. Kallioras, A.A. Correia, F. Graziotti, A. Penna, G. Magenes, Collapse shake-table testing of a clay-URM building with chimneys, Bull. Earthq. Eng. 18 (2020), https://doi.org/10.1007/s10518-019-00730-0.
[88] F. Graziotti, U. Tomassetti, S. Kallioras, A. Penna, G. Magenes, Shaking table test on a full scale URM cavity wall building, Bull. Earthq. Eng. 15 (2017), https://doi.org/10.1007/s10518-017-0185-8.
[89] K.L. Su R, Typical collapse modes of confined masonry buildings under strong earthquake loads, Open Construct. Build Technol. J. 5 (2011), https://doi.org/10.2174/1874836801105010050.

[90] R. Ceravolo, E. Matta, A. Quattrone, L. Zanotti Fragonara, Amplitude dependence of equivalent modal parameters in monitored buildings during earthquake swarms, Earthq. Eng. Struct. Dynam. 46 (2017), https://doi.org/10.1002/eqe.2910.
[91] S. Lagomarsino, A. Penna, A. Galasco, S. Cattari, TREMURI program: an equivalent frame model for the nonlinear seismic analysis of masonry buildings, Eng. Struct. 56 (2013), https://doi.org/10.1016/j.engstruct.2013.08.002.
[92] V. Bernardo, S. Karimzadeh, D. Caicedo, S.M.S. Hussaini, P.B. Lourenço, Fragility-based seismic assessment of traditional masonry buildings on azores (portugal) using simulated ground-motion records, Earthq. Spectra 40 (2024) 2836–2861.
[93] N.S. Kwong, A.K. Chopra, A generalized conditional mean spectrum and its application for intensity-based assessments of seismic demands, Earthq. Spectra 33 (2017) 123–143.
[94] P. Jayarajan, Application of conditional mean spectrum in the seismic assessment of a braced frame steel structure. IOP Conference Series: Materials Science and Engineering vol. 936, IOP Publishing, 2020 012030.